

# Entropy production, dynamical localization and criteria for quantum chaos in the open quantum kicked rotor

**Paul A. Miller and Sarben Sarkar**

Department of Physics, King's College London, Strand, London WC2R 2LS, UK

**Abstract.**

The von Neumann entropy production for a quantum mechanical kicked rotor coupled to a thermal environment is calculated. This rate of entropy increase is shown to be a good criterion to distinguish between quantum mechanical counterparts of chaotic and regular classical motion. We show that for high temperatures the entropy production rate increases linearly with the Kolmogorov-Sinai entropy of the classical system. However, for lower temperatures we also show that there are fluctuations in this linear behaviour due to dynamical localization.

PACS numbers: 05.45.+b, 03.65.-w

Short title: Entropy, localization and quantum chaos

June 19, 2018

## 1. Introduction

The investigation of the quantum mechanical behaviour of systems with classically chaotic counterparts is a rich and exciting field of study. Many beautiful results have been found over the years regarding the semiclassical quantization of nonintegrable systems [1, 2, 3] and “quantum chaology” [4, 5, 6]. A major component of the approach involves the study of eigenvalue statistics, eigenfunction “scarring” etc. Classical chaotic behaviour, however, by definition a dynamical phenomenon, seems to be suppressed at the quantum level [7, 8]. Apart from a brief time, during which its behaviour effectively mimics the classically chaotic dynamics, the quantized version of a bounded and conservative classical system is quasiperiodic and, therefore, predictable [9, 10].

Chaotic systems thus test our understanding of the relationship between classical and quantum mechanics. If classical behaviour is not a naturally emergent property of such systems in the absence of explicit measurements then it is natural to consider the effect of environments on the quantum system [11]. Quantum mechanical interference and superpositions, the cause of the aforementioned discrepancy, can be shown to be destroyed on extremely short timescales, in tractable model systems, by opening these systems to environmental influences [12, 13]. Some features of classical behaviour can then emerge without having to take the semi-classical limit.

Zurek and Paz [14] have used the exactly solvable, inverted harmonic oscillator to model heuristically unstable chaotic motion near a hyperbolic point, although this system is certainly not chaotic itself. The Hamiltonian for this model is

$$H(x, p) = \frac{p^2}{2} - \frac{\lambda^2 x^2}{2}. \quad (1)$$

The effect of the the environment on this system might be expected to provide clues to the behaviour that might be observed if we were to open a chaotic system in a similar manner. The oscillator can be described by a master equation in the position basis. Choosing the bath as a collection of harmonic oscillators in thermal equilibrium at high temperature, with an Ohmic spectral density proportional to a *small* dissipation parameter, simplifies this equation enormously. Analysing the time evolution of an initial minimum uncertainty state using this equation, Zurek and Paz have found that the von Neumann entropy,  $S(t)$ , quickly begins to increase linearly in time with a rate set by the quantity,  $\lambda$  in equation (1),

$$\dot{S}(t) \equiv h_Q = \lambda. \quad (2)$$

Recently, however, we have generalized this result [15] by considering the entropy production for all temperatures and for non-negligible dissipation parameters,  $\gamma_{diss}$ . We found that equation (2) is modified to

$$\dot{S}(t) \equiv h_Q = \sqrt{\lambda^2 + \gamma_{diss}^2} - \gamma_{diss}, \quad (3)$$

but reduces to it when  $\gamma_{diss} \ll \lambda$ , as required.

As  $\lambda$  is loosely analagous to the Lyapunov exponent of a chaotic system, Zurek and Paz conjecture that the entropy production rate might differentiate between chaotic and regular systems, and that this rate will also be determined by the (positive) Lyapunov exponent of the classical system. From the Alekseev-Brudno theorem (see p.4 in [1], also [16])

$$\lim_{t \rightarrow \infty} \frac{I(t)}{t} = h_{KS} = \sum \Lambda^+, \quad (4)$$

where  $I(t)$  is the Shannon entropy,  $h_{KS}$  is the Kolmogorov-Sinai entropy - a measure of the average rate at which a classical system will lose information [16] - and the sum is over all the local positive Lyapunov exponents,  $\{\Lambda^+\}$ , in phase space. From this definition, of course, it is clear that  $h_{KS}$  is actually an entropy *rate*. Consequently we will modify the Zurek and Paz conjecture to the statement that  $\dot{S}(t)$  increases *linearly* with  $h_{KS}$ . This has the attractive feature of dealing both in the classical and quantum mechanical cases with the change of entropy in time. Furthermore, the equality in equation (2) has been replaced with the weaker statement of linear increase. This is the conjecture that we will consider throughout the rest of our discussion.

The idea that quantum systems can be defined as “chaotic” or “regular”, depending on their behaviour under a perturbed evolution, is appealing and an old one [11]. An approach similar in spirit is due to Schack and Caves [17], who have recently considered perturbed quantum maps in an information theoretic framework and have established a criterion for chaos known as “hypersensitivity to perturbation”. In this paper we will study the prototypical, theoretically important [18, 19] and experimentally realizable [20, 21] quantum kicked rotor. However, we will consider the dynamics under the influence of a tractable, model environment and seek to find evidence for the modified conjecture when the parameters of the combined system are compatible with those assumed during the framing of the conjecture.

The plan for the paper is as follows. In Section 2 we shall briefly outline the features of the classical and quantum kicked rotor relevant to the present study. In Section 3 we will derive the one-step propagators for both the (reduced) density matrix of the rotor and its associated Wigner function representation. The latter result allows us to see clearly that by opening the system we still have a quantum analogue of the classical kicked rotor, or rather its standard map. Also in this section we endeavour to quantify the effect of the environment on the coherence of the system.

The results from our numerical analysis follow in Section 4 wherein we will produce firm evidence in favour of the use of entropy production as a criterion for quantum chaos *and* of the modified conjecture, at least in the parameter ranges considered. We will also suggest explanations for those features found not to be in accordance with the conjecture. The conclusions follow in Section 5.

## 2. The Kicked Rotor

The kicked rotor model has been used extensively in studies of classical chaos and its quantum manifestations [10, 11, 18, 19, 22, 25]. Consequently the literature is vast, but for convenience we outline here those features of its complex behaviour necessary for an understanding of our model and results. Even for readers familiar with the model a perusal would be useful in order to establish the notation used.

### 2.1. Classical Features

The system Hamiltonian with which we will deal is that of a periodically kicked rotor,

$$H_{rotor} = \frac{p^2}{2} - \frac{K}{4\pi^2} \cos(2\pi q) \sum_{n=-\infty}^{+\infty} \delta(t - n), \quad (5)$$

where  $p$  is an angular momentum and  $q$  is a scaled angle variable. Integrating the equations of motion from immediately after a delta function "kick" to just after the next such kick will give a version of the famous *standard map*

$$\begin{aligned} p_{n+1} &= p_n - \frac{K}{2\pi} \sin 2\pi q_{n+1}, \\ q_{n+1} &= (q_n + p_n) \pmod{1}. \end{aligned} \quad (6)$$

The map is periodic, with period 1, in both directions of phase space - in the angle direction by definition and in the momentum direction due to the form of the map. This means that one can simply view trajectories projected back onto the unit square,  $[0, 1) \times [0, 1)$ , in order to study the dynamics for different initial conditions. However, even though there is periodicity in the momentum direction, the momentum is actually defined on the infinite interval  $[-\infty, \infty]$ . The phase space has, therefore, the topology of a cylinder.

The nonlinearity of the map is controlled by strength of the kick,  $K$ . The trivial, regular motion when  $K = 0$ , becomes more and more complicated as  $K$  is increased [18, 19]. When  $K < K_c \approx 0.97\dots$  some KAM tori span the cylinder and prevent diffusion in the momentum direction. As  $K$  increases still further these tori are destroyed, allowing the momentum to diffuse, i.e.

$$\langle (p(n) - p(0))^2 \rangle = D(K)n, \quad (7)$$

at a rate determined by the diffusion constant,  $D(K)$ . Here, the averaging is over a distribution of initial conditions. The diffusion constant can be calculated analytically [19, 23], and it is found that correlations in the angle variable from kick to kick influence its form considerably. If we ignore such correlations - an increasingly accurate approximation as  $K \rightarrow \infty$  - the angle variable can be assumed to be randomly but

uniformly distributed on the unit interval. This *quasilinear* approximation allows us to write

$$D_{ql}(K) = \frac{1}{2} \left( \frac{K}{2\pi} \right)^2. \quad (8)$$

Inclusion of these dynamical correlations leads to corrections which decrease in magnitude as  $K$  gets larger, i.e. it is found [19, 23]

$$D(K) = \frac{1}{2} \left( \frac{K}{2\pi} \right)^2 \left( 1 - 2J_2 \left( \frac{K}{2\pi} \right) + 2 \left( J_2 \left( \frac{K}{2\pi} \right) \right)^2 + \dots \right), \quad (9)$$

where  $J_2$  denotes a Bessel function of order 2.

For all finite values of  $K$ , KAM tori remain around elliptic points in phase space, of which there are an infinite number. These stable islands, surrounded by a chaotic sea, characterize what is known as a “mixed” phase space, meaning that two nearby trajectories either remain “near” to one another for all time or diverge exponentially, depending on whether they are to be found in a regular region or a chaotic one, respectively (See figures [1] and [2]). Hence the Lyapunov exponents for the system are dependent on the starting point in phase space, but gradually converge to a uniform value as  $K \rightarrow \infty$ .

From Pesin’s theorem [24], the kicked rotor, being a chaotic system with one degree-of-freedom, possesses a positive *KS entropy*,  $h_{KS}$ , which will be equal to its positive Lyapunov exponent for  $K$  sufficiently large. Chirikov [22] has calculated this quantity and found

$$h_{KS} \approx \ln \left( \frac{K}{2} \right). \quad (10)$$

## 2.2. Quantum Features

The periodicity of the angle variable gives rise to a numerable and discrete set of momentum eigenvalues defined by

$$\hat{p}|l\rangle = p_l|l\rangle = 2\pi\hbar l|l\rangle, \quad (11)$$

where  $l$  is an integer. The corresponding eigenstates are obviously eigenstates too of the kinetic energy operator  $\hat{H}_0 = \hat{p}^2/2$ , and we write

$$\hat{H}_0|l\rangle = E_l|l\rangle = 2\pi^2\hbar^2 l^2|l\rangle. \quad (12)$$

The Hamiltonian of equation (5) leads to a one-step unitary transformation

$$U(t_{n+1}, t_n) = U_k U_f, \quad (13)$$

which defines the quantum standard map. Here,  $t_n$  is the time after the  $n$ th kick and  $U_k$  is the unitary kick evolution operator. It can be written in the momentum representation as

$$\langle l'|U_k|l\rangle = i^{l'-l} J_{l'-l}(K/4\pi^2\hbar), \quad (14)$$

with  $J_m$  denoting a Bessel function of integer order  $m$ .  $U_f$  is the operator corresponding to unitary free rotation between the delta function kicks, and has the momentum representation

$$\langle l' | U_f | l \rangle = \exp(-i2\pi^2 \hbar l^2) \delta_{l'l}. \quad (15)$$

The unitary dynamics was first investigated by Casati et al. [10] using initial states highly localized in momentum. It was found that  $\langle (\hat{p}(n) - \hat{p}(0))^2 \rangle$  shows diffusive behaviour in approximate agreement with the classical case, but only up to a finite *break* time,  $n^*$ , after which the momentum ceases to grow further and quasiperiodic motion around some finite average is found. This defines a *localization length* via

$$\overline{\langle (\hat{p}(n) - \hat{p}(0))^2 \rangle} = (2\pi\hbar)^2 L^2, \quad (16)$$

for  $n > n^*$ . Good analytic and numerical evidence now exists pointing to the fact that the eigenstates of the unitary evolution operator of equation (13) above are localized in momentum and have essentially discrete spectra on the unit circle of the complex plane. These assumptions lead to the following estimates for  $L$  and  $n^*$  [30]

$$L \approx \left( \frac{D(K)}{2\pi^2 \hbar^2} \right), \quad (17)$$

and

$$n^* \approx 2L. \quad (18)$$

It is important to note that both quantities are inversely proportional to the square of the scaled unit of action,  $\hbar$ . We also note that *classical* correlations, which can both increase and decrease the diffusion constant from its quasilinear value,  $D_{ql}$ , (see equations (8) and (9)) can also directly affect the quantum dynamics via this localization mechanism.

The discrepancy between the classical and quantum diffusive behaviour of the kicked rotor is therefore known to be a consequence of quantum interference. If the phase coherence could somehow be destroyed one might expect to recover the classical diffusion. Various authors have considered this problem [11, 26, 27, 30] and have examined the effect of an environment on localization. However, previously the relationship between the classical and quantum entropy production, the former being a quantitative measure of chaos, has *not* been studied. This approach is important since we have growing evidence that it is a generic one.

### 3. Open Dynamics

We now proceed to derive the propagator for the density matrix of the rotor after tracing out the environmental degrees of freedom, i.e. the propagator for the *reduced* density matrix. This will enable us to calculate the von Neumann entropy at each time step, upon iteration of an arbitrary initial state.

### 3.1. The Reduced Density Matrix Propagator

We will restrict attention to the situation *between* kicks initially and consider the free rotor to be coupled through its momentum to a thermal bath of harmonic oscillators. The Hamiltonian for this system,

$$H = \frac{p^2}{2} + \sum_k \left( \frac{p_k^2}{2m_k} + \frac{m_k \omega_k^2 q_k^2}{2} \right) + p \sum_k c_k q_k, \quad (19)$$

can be written as

$$H = \frac{p^2}{2} + \sum_k \hbar \omega_k (b_k^\dagger b_k + \frac{1}{2}) + p \sum_k \bar{c}_k (b_k^\dagger + b_k), \quad (20)$$

where  $\bar{c}_k = \sqrt{\hbar/(2m_k \omega_k)} c_k$  is a renormalized coupling and

$$b_k = \sqrt{\frac{m_k \omega_k}{2\hbar}} \left( q_k + i \frac{p_k}{m_k \omega_k} \right),$$

$$b_k^\dagger = \sqrt{\frac{m_k \omega_k}{2\hbar}} \left( q_k - i \frac{p_k}{m_k \omega_k} \right).$$

As  $[q_j, p_k] = i\hbar \delta_{jk}$ , these annihilation and creation operators satisfy  $[b_j, b_k^\dagger] = \delta_{jk}$ .

We choose an uncorrelated initial product state

$$\rho(0) = \rho^S(0) \otimes \prod_k \rho_{th}^k, \quad (21)$$

where  $\rho_{th}^k$  is the density matrix of the  $k$ th harmonic oscillator in thermal equilibrium at temperature  $T$ , defined by

$$\rho_{th}^k = \left[ 1 - \exp \left( -\frac{\hbar \omega_k}{k_B T} \right) \right]^{-1} \sum_n \exp \left( \frac{-n \hbar \omega_k}{k_B T} \right) |n\rangle \langle n|. \quad (22)$$

To specify the problem further we also need to choose a physically reasonable environmental *spectral density* [29],  $I(\omega)$ , defined formally by

$$I(\omega) = \sum_k \delta(\omega - \omega_k) \frac{c_k^2}{2m_k \omega_k}. \quad (23)$$

More generally, if we assume every environmental oscillator to have equal mass, we can write [13]

$$I(\omega) \approx S(\omega) \frac{c^2(\omega)}{2m\omega}, \quad (24)$$

with a smooth density  $S$ . In order to avoid the influence of unphysical, extremely high frequencies we assume the existence of an upper, or cutoff frequency,  $\omega_c$ , and choose a continuum of oscillators distributed according to the density

$$S(\omega) c^2(\omega) = 2m\eta \omega^q \exp\left(-\frac{\omega}{\omega_c}\right), \quad (25)$$

with  $q > 1$ , which reduces to that used by Caldeira and Leggett [29] when we choose a so-called *Ohmic* environment with  $q = 2$ . Hamiltonians and initial conditions of this Ohmic type have been considered by Jiushu et al. in [33] and the *exact* time evolution for the reduced density matrix has been obtained. We proceed along similar lines but consider the general case with  $q > 1$  being the only assumption. We arrive finally at an expression for the reduced density matrix of the rotor in the momentum representation

$$\langle m | \rho^S(t) | n \rangle = \exp \left( -\frac{i}{\hbar} (E_m - E_n)(t + A(q, t)) - \frac{(p_m - p_n)^2}{\hbar} B(q, t) \right) \langle m | \rho^S(0) | n \rangle. \quad (26)$$

The environmental terms in this expression, given by  $A(q, t)$  and  $B(q, t)$ , have been evaluated explicitly for all  $q > 1$  [34]. The expressions are particularly simple, however, for the Ohmic case, and we concentrate on this important case from here on. We find

$$A(2, t) = 2\eta(\arctan(\omega_c t) - \omega_c t), \quad (27)$$

and

$$B(2, t) = \frac{\eta}{2} \ln(1 + \omega_c^2 t^2) + \eta \ln \prod_{j=1}^{\infty} \left( 1 + \left( \frac{\omega_c t}{1 + j\beta\hbar\omega_c} \right)^2 \right), \quad (28)$$

where the usual notation of  $\beta = 1/(k_B T)$  has also been used.

There are a few points to note here. Firstly, were  $K = 0$  in equation (5), then equation (26) would describe fully the time evolution of any initial state,  $\rho^S(0)$ , in the momentum representation, for a classically *nonchaotic* rotor. Secondly, we return to the correct unitary dynamics, corresponding to conservative evolution of the rotor, when  $\eta$  is set to 0. (This amounts to setting all coupling constants,  $c_k$ , to zero.) Finally, we will consider equation (26) to describe the time evolution of the quantum kicked rotor between kicks and so will set  $t = 1$  in equations (26), (27) and (28). The heat bath is assumed to be sufficiently large to remain in thermal equilibrium as it interacts with the system between each kick. For this assumption to be valid the coupling constants,  $\{c_k\}$ , are taken to be *small*. Hence, for the spectral density in equation (25),  $\eta \ll 1$ , a common assumption [14, 30].

The system evolution, from just after the kick at  $t = n$  until just *before* the kick at  $t = n + 1$ , where  $n$  is an integer, is given by a master equation of the form

$$\langle l' | \rho^-(n+1) | m' \rangle = \sum_{l, m} G^f(l', m', l, m) \langle l | \rho^+(n) | m \rangle, \quad (29)$$

where

$$G^f(l', m', l, m) = G_C^f(l', m', l, m) \Gamma(l, m), \quad (30)$$

$G_C^f(l', m', l, m)$  is the unitary summation kernel given by

$$G_C^f(l', m', l, m) = \exp\left(-\frac{i}{\hbar}(E_l - E_m)\right) \delta_{l'l} \delta_{m'm} \quad (31)$$



and

$$\Gamma(l, m) = \exp\left(-\frac{i}{\hbar}(E_l - E_m)A(2, 1) - \frac{(p_l - p_m)^2}{\hbar}B(2, 1)\right) \quad (32)$$

describes the non-unitary influence of the environment on the dynamics.

It is assumed that during each kick both free evolution and the influence of the environment are negligible. We are then led formally to the summation kernel for the kick, defined by the master equation

$$\langle l' | \rho^+(n+1) | m' \rangle = \sum_{l, m} G^k(l', m', l, m) \langle l | \rho^-(n+1) | m \rangle. \quad (33)$$

Choosing now the shorthand notation used by Dittrich and Graham [32] of  $k := K/4\pi^2\hbar$  and  $b_m(x) := i^m J_m(x)$  we can write explicitly

$$G^k(l', m', l, m) = b_{l'-l}(k) b_{m'-m}^*(k). \quad (34)$$

Even as the density matrix evolves, according to master equations (29) and (33) above, it must, of course, remain normalized, hermitian and positive [31]. These properties in turn impose conditions on the kernels of equations (30) and (34) which can easily be shown to hold [34], implying that the evolution of the reduced quantum statistical density operator is a valid one.

The one time-step evolution of the density matrix is now simply the convolution of  $G^f$  and  $G^k$  defined in equations (30) and (34) above, respectively, and it is easily confirmed that

$$\langle l' | \rho^+(n+1) | m' \rangle = \sum_{l, m} G(l', m', l, m) \langle l | \rho^+(n) | m \rangle, \quad (35)$$

where

$$G(l', m', l, m) = G_C(l', m', l, m) \Gamma(l, m), \quad (36)$$

in which

$$G_C(l', m', l, m) = \langle l' | U | l \rangle \langle m | U^\dagger | m' \rangle \quad (37)$$

is the unperturbed, unitary propagator. When there is no environment, i.e. as  $\eta \rightarrow 0$ , then  $\Gamma(l, m) \rightarrow 1$  for each  $l$  and  $m$ .

### 3.2. Destruction of Coherence

It was stated above that the term  $\Gamma(l, m)$  in equation (36) makes a non-unitary contribution to the dynamics. In this section we would like to quantify this statement.

A measure of decoherence is the decay probability,  $P_1$ , of a quasienergy eigenstate in a single timestep. In order to calculate  $P_1$  we first consider the probability of transition,

$P^1(s|r)$ , from an quasienergy eigenstate  $|r\rangle$  to a quasienergy eigenstate  $|s\rangle$  in a single timestep. In fact, if  $\rho^+(0) = |r\rangle\langle r|$  then we may write

$$P^1(s|r) = \langle s|\rho^+(1)|s\rangle. \quad (38)$$

The propagator in the quasienergy representation is therefore required, and the master equation (35) maybe be rewritten

$$\langle \alpha_1|\rho^+(n+1)|\beta_1\rangle = \sum_{\alpha_0, \beta_0} G^{qe}(\alpha_1, \beta_1, \alpha_0, \beta_0) \langle \alpha_0|\rho^+(n)|\beta_0\rangle, \quad (39)$$

where

$$U|\alpha_0\rangle = e^{i\phi_{\alpha_0}}|\alpha_0\rangle, \quad (40)$$

and similarly for  $|\alpha_1\rangle, |\beta_0\rangle$  and  $|\beta_1\rangle$ . One easily finds

$$G^{qe}(\alpha_1, \beta_1, \alpha_0, \beta_0) = \sum_{l,m} e^{i(\phi_{\alpha_1} - \phi_{\beta_1})} \langle \alpha_1|l\rangle \langle l|\alpha_0\rangle \langle \beta_0|m\rangle \langle m|\beta_1\rangle \Gamma(l, m). \quad (41)$$

Thus, because of equations (38) and (39), we find

$$\begin{aligned} P^1(s|r) &= G^{qe}(s, s, r, r) \\ &= \sum_{l,m} \langle s|l\rangle \langle l|r\rangle \langle r|m\rangle \langle m|s\rangle \Gamma(l, m). \end{aligned} \quad (42)$$

We can now use this expression to calculate  $P_1$  by summing over all possible final states,  $|s\rangle$  (different from  $|r\rangle$ ) and averaging over the various possible initial states (see, for example, reference [27]):

$$P_1 = \frac{1}{D} \sum_{\substack{r,s \\ (r \neq s)}} P^1(s|r), \quad (43)$$

where  $D$  is the dimension of the truncated basis (See Section 4). Inserting equation (42) and using the fact that

$$\sum_{\substack{s \\ (r \neq s)}} \langle s|l\rangle \langle m|s\rangle = \delta_{m,l} - \langle r|l\rangle \langle m|r\rangle \quad (44)$$

we find

$$P_1 = 1 - \frac{1}{D} \sum_r \gamma_r, \quad (45)$$

where we have defined

$$\gamma_r = \sum_{l,m} |\langle r|l\rangle|^2 |\langle r|m\rangle|^2 \Gamma(l, m). \quad (46)$$

We may estimate this expression analytically [34] if we assume that *every* quasienergy eigenfunction is exponentially localized according to

$$|\langle r|l\rangle|^2 \approx \exp\left(-\frac{|l - l_r|}{L}\right). \quad (47)$$

Here we have denoted the centre of localization by  $l_r$  and  $L$  is the localization length defined previously in equation (17). However, not every such eigenstate has this structure, as certain “double-hump” quasienergy eigenstates exist, so-called because they have two localization centres.

For accuracy therefore, we have calculated  $P_1$  numerically and examined the effect changing  $K$ ,  $\hbar$  and  $\beta$ , the environmental inverse temperature. We present our results in Section 4.

### 3.3. The Wigner Distribution Propagator

We would like now to examine the classical limit of our system. To do so we choose to work in the Wigner representation for a phase space with the topology of a cylinder. The notation in this section is exactly that used in refs.[31, 32], in the latter of which this representation is succinctly described.

The Wigner distribution on our cylindrical phase space at time  $n$ ,  $W_n(q, p)$ , consists of  $\delta$ -functions concentrated on the definite values of momentum,  $p = \pi\hbar l$ , for  $l$  an integer. One therefore writes

$$W_n(q, p) = \sum_l W_n^{(l)}(q) \delta(p - \pi\hbar l) \quad (48)$$

for the Wigner distribution at this time. Its (one) time-step generator,  $G_W$ , is defined by

$$W_{n+1}^{(\bar{l})}(\bar{q}) = \sum_l \int_0^1 dq G_W(\bar{l}, \bar{q}, l, q) W_n^{(l)}(q), \quad (49)$$

and can be expressed in terms of the one-step density matrix propagator, most conveniently in the momentum representation, using

$$G_W(\bar{l}, \bar{q}, l, q) = \sum_{m_1, m_2} \sum_{l_1, l_2} \delta_{\bar{l}, m_1 + m_2} \delta_{l, l_1 + l_2} \exp\{2\pi i[(m_1 - m_2)\bar{q} - (l_1 - l_2)q]\} \\ \times G(m_1, m_2, l_1, l_2). \quad (50)$$

It will be convenient to make the transformation from the density matrix propagator to the Wigner function propagator for both the free and the kicked part separately. A convolution of the two will then yield the desired quantized map in the Wigner function representation.

Use of equation (30) in equation (50) gives

$$G_W^f(\bar{l}, \bar{q}, l, q) = \delta_{\bar{l}l} \text{Ga}(x, \Delta, 1), \quad (51) \\ \equiv \delta_{\bar{l}l} \sum_{k=-\infty}^{\infty} \exp\left(2\pi i k x - 2\pi^2 k^2 \Delta\right),$$

i.e., proportional to a periodic Gaussian with period 1. Here,  $x$  and  $\Delta$  are defined by

$$x = \bar{q} - q - \pi\hbar\bar{l}(1 + A(1)), \quad (52)$$

and

$$\Delta = 2\hbar B(1). \quad (53)$$

This periodic Gaussian reduces to a periodic  $\delta$ -function with the argument  $\bar{q} - q - \pi\hbar\bar{l}$  for  $\eta \rightarrow 0$ , as expected. Similarly, use of equation (34) in equation (50) gives

$$G_W^k(\bar{l}, \bar{q}, \bar{l}, \bar{q}) = i^{\bar{l}-\bar{l}} \exp\{2\pi i \bar{l}(\bar{q} - \bar{q})\} J_{\bar{l}-\bar{l}}(2k \sin(2\pi\bar{q})) \sum_m \exp\{-4\pi i m(\bar{q} - \bar{q})\}. \quad (54)$$

There remains only to convolute the two propagators to give

$$\begin{aligned} G_W(\bar{l}, \bar{q}, l, q) &= \sum_{\bar{l}} \int_0^1 d\bar{q} G_W^k(\bar{l}, \bar{q}, \bar{l}, \bar{q}) G_W^f(\bar{l}, \bar{q}, l, q) \\ &= J_{\bar{l}-l}(2k \sin(2\pi\bar{q})) \text{Ga}(\bar{q} - q - \pi\hbar l(1 + A(1)), 2\hbar B(1), 1). \end{aligned} \quad (55)$$

When  $\eta \ll 1$  and  $\hbar \rightarrow 0$  this quantum map can be shown [35] to reduce to the classical map of equation (6), as required.

#### 4. Results

We now present the results of our numerical calculations. For each run we began with an initial coherent state centred at some point  $(p, q)$  in phase space. We choose Planck's constant,  $h$  to be a rational multiple of

$$\gamma := \frac{1}{\sqrt{5}-1}. \quad (56)$$

This avoids any resonances [18], which might occur between the frequency of the driving force and those frequencies associated with the energy levels,  $\{E_n\}$ , of the unperturbed, regular rotor for rational  $h$ . (Such resonances give rise to a superdiffusive, quadratic increase of the rotor's energy with time in contrast to the linear increase found for the classical rotor.) The infinite dimensionality of the Hilbert space forces us to truncate the momentum basis in which we work. We have chosen, for the generation of the results presented below, to use a truncated basis set which is symmetric about the zero momentum eigenstate. That is, we have used the set  $\{|-n\rangle, |-n+1\rangle, \dots, |-1\rangle, |0\rangle, |1\rangle, \dots, |n-1\rangle, |n\rangle\}$ , where  $n$  was chosen large enough to keep the density matrix normalized to an accuracy of better than 1 part in  $10^7$ ; i.e.

$$\text{Tr} [\rho_S(t)] = 1, \quad (57)$$

for the time of interest. Typically,  $n$  ranged from  $\approx 250$  up to  $\approx 450$ , depending on the parameter values used.

A propagation through one time step was then effected by computing equation (29) followed by equation (33). At each stage the von Neumann entropy,  $S(t)$  was calculated by using the approximation

$$S(t) := -\text{Tr} [\rho_S(t) \ln \rho_S(t)] \approx - \sum_{i=-n}^n \lambda_i \ln \lambda_i, \quad (58)$$

where  $\{\lambda_i | -n \leq i \leq n\}$  is the set of eigenvalues of the density matrix  $\rho_S(t)$  at that time. The entropy is a maximum if and when each  $\lambda_i = 1/(2n+1)$ , giving an upper limit to the entropy of  $S_{max} = \ln(2n+1)$  as a result of the truncation.

Finally, as we wish to investigate the modified conjecture it is reasonable to make the same characterisation for our environment as Zurek and Paz [14]. The spectral density is Ohmic but a high temperature environment is also required. Consequently, the parameters are chosen so that  $k_B T > \hbar \omega_C$ .

#### 4.1. Qualitative Comparisons

**4.1.1. Local KS Entropy** When the nonlinearity parameter,  $K$ , of our rotor is greater than or equal to 6 there are no discernable stable islands in phase space plots of the classical standard map. They do still exist, of course, but the fraction of the unit square they occupy at these values is small. In such a situation the variation in the Lyapunov exponent will be small throughout phase space and the inverted oscillator model will be more likely to be considered adequate. However, when the value of  $K$  is so small as to allow KAM islands to exist and occupy a significant fraction of phase space we must expect the *local* Lyapunov exponents to vary considerably. All of these local Lyapunov exponents contribute to the sum in the calculation of the *global* KS entropy in equation (4). However, we can also define a *local* KS entropy by *restricting* the sum over local Lyapunov exponents to those corresponding to the points in an initial classical probability distribution. Thus, in view of the aim of this investigation, we might expect that the rate of von Neumann entropy increase will depend strongly upon precisely where in a mixed space we locate an initial coherent state, i.e. upon the local KS entropy corresponding to its classically analogous initial probability distribution.

To illustrate the usefulness of the local KS entropy concept we considered first of all the time evolution of two initially Gaussian, symmetric probability distributions in phase space, one centred in a classically regular region when  $K = 1$ , with the other centred in a chaotic region for the same  $K$  value. The variance of these distributions was chosen as  $\hbar/2$  in order to render them classical analogues of the minimum uncertainty quantum initial states to which their evolutions will be compared.

In figures [1] and [2] we plot the result of taking 100 sample points from each of these distributions and plotting the first 300 points of the classical trajectories corresponding to each such point. The regularity of the dynamics in figure [1], where the initial state is

centred at  $(0.0, 0h)$ ,  $h$  being Planck's constant as before, can be compared to the chaotic trajectories in figure [2] resulting from the initial state being centred at  $(0.5, 2h)$ .

Our next step is to calculate the KS entropy [22] corresponding to each of the points used to sample the Gaussians and then to take the average. This we define as the local KS entropy corresponding to the initial states. The calculations are done for a range of  $K$  values from 0 to 6 giving rise to progressively less mixed phase spaces. In figure [3] we see that this *local* KS entropy differs greatly for these two states when  $1 \leq K \leq 4$ , i.e. after a significant number of invariant KAM curves have been destroyed and before the  $K$  value at which the KAM island surrounding the elliptic fixed point at the origin disappears completely from phase space plots [18, 22]. As  $K$  increases further these local KS entropies agree more and more, and can be well approximated by the *global* KS entropy [22] of equation (10).

*4.1.2. Local Quantum-Classical Entropy Correspondence* Though global KS entropy can, of course, be defined for *all* values of  $K$ , it must be numerically determined when a largely mixed phase space prevails. We show here, however, that it is not the quantity to be used in any prediction of the quantum mechanical entropy production rate. The correct quantity is the local KS entropy.

To show this we next considered the quantum mechanical time evolution of the two coherent states analogous to the two classical distributions used above. For each state we have calculated the von Neumann entropy production rate over 20 time steps and for the set  $K = 1, 2, \dots, 5$ , values at which the locally calculated KS entropies differ greatly (See figure [3]). The results corresponding to the initial, classically regular state centred at  $(0.0, 0h)$  can be seen in figure [4] and those corresponding to the (classically chaotic) state centred at  $(0.5, 2h)$  can be seen in figure [5]. In the former case the entropy production rates reflect very well the local KS entropy values of figure [3]. The initially low values of each, when  $K = 1, 2$ , increase when  $K = 3$ , once more when  $K = 4$ , and finally jump dramatically when  $K = 5$ . However, the situation for the coherent state situated initially in a classically chaotic region of phase space is strikingly different. Indeed, the steady increase in plateau height with  $K$  mirrors well the local KS entropy of figure [3] as it, too, increases steadily with  $K$ . No sudden jumps are apparent, and only when  $K = 5$  do the entropy production rates of both initial states approach one another, just as they do classically.

*4.1.3. Overlap Effects in a Mixed Phase Space* Entropy production, thus, *does* depend on where we initially place our coherent state but we expect this variability to decrease with increasing values of  $K$  as the classical phase space becomes more uniformly chaotic. However, the initial states for  $K = 1$  we have considered above have been well localized (figures [1] and [2]) in either entirely regular or entirely chaotic regions,

with no significant overlap with nearby regions which may have very different classical behaviour. In order to investigate the effect significant overlaps have on the rate of entropy production we set  $K = 4$ , where, as can be seen from the classical phase space plot of figure [6], one large regular region still exists in a sea of chaotic trajectories. If we locate our initial coherent states along the diagonal which intercepts this KAM island, with their centres equally spaced at  $(0, 0), (h, h), (2h, 2h), \dots$ , we find an interesting feature. The rate of entropy increase is lower when the initial state overlaps the regular region and only when a significant overlap exists initially with the chaotic sea does the entropy begin to increase at the robust rate which is found for all the states with little or no overlap with this island. Classically we see analogous behaviour once more if we examine the locally averaged KS entropy for initial distributions which correspond in their mean and variance to those quantum states of figure [7]. We show the results of this calculation in figure [8]. Here, as in the quantum case, an asymptotic approach to a constant KS entropy value (of  $\approx 0.8$ ) is found as the initial distribution overlaps to a lesser degree with the stable KAM island.

It seems, therefore, that entropy production is indeed a suitable criterion by which to distinguish between regular and chaotic motion. Recently Zarum and Sarkar [36] produced qualitative evidence in support of this claim for the kicked rotor model. They quantized on a torus and perturbed the rotor in a different, but noisy and non-unitary way, leading to an entropy increase. Initial coherent states uniformly distributed on the torus gave rise to a corresponding distribution of (constant) entropy production rates which reflect in a remarkable way the classical KS entropy profile for initial points in a mixed phase space. Similar results have recently been obtained for the quantum kicked top model [37].

## 4.2. Quantitative Comparisons

The *quantitative* analysis of the relation between  $h_Q$  and  $h_{KS}$  has been the goal of this paper and we now turn our attention to it.

*4.2.1. Temperature-induced Correspondence* Firstly we examine the effect that increasing the environmental temperature has on quantum-classical correspondence. To do so we have once more iterated in time a normally distributed initial classical state consisting of 25000 points. The distribution was chosen to be centred at the same point, and to have the same variance, as a minimum uncertainty quantum state centred at  $(0.5, h)$ . We have chosen  $h = 0.1\gamma$  and  $K = 3$  to examine the correspondence in time between the classical average value and the quantum expectation value of the squared momentum variable in figure [9]. Clearly, the classical behaviour, marked with stars (\*), is approached to a greater degree as the temperature is increased (equivalently, as

$\beta = 1/k_B T$  is decreased) despite the fact that  $\hbar$  remains fixed.

Now, in figure [10] we examine, for the same parameters, the consequences for the rate of von Neumann entropy production and in figure [11] the consequences for the von Neumann entropy itself. The truncated basis chosen for these runs as  $\{|-n\rangle, |-n+1\rangle, \dots, |-1\rangle, |0\rangle, |1\rangle, \dots, |n-1\rangle, |n\rangle\}$ , where  $n = 250$ . This implies a maximum entropy value of  $\ln 501 \approx 6.2$ .

For inverse temperatures  $\beta = 1.00, 0.10$  and  $0.01$ , and for the time regime shown, we find that the von Neumann entropy is not near enough to the saturation value for the linearity of its increase with time to be affected. Eventually, however, the entropy will begin to saturate even for these low temperatures and the rates of entropy increase will fall below that of their respective “plateaux” shown in figure [10]. A feature *not* expected on the basis of the inverted oscillator model [14, 15], and yet clearly in evidence here, is the dependence on temperature of the plateau height. Hence the need for a *modified* conjecture to take this effect into account.

When we increase the temperature still further, so that  $\beta = 0.001$ , we note two generic features. Firstly, the time at which the approximately constant entropy production is attained, i.e. the time at which the plateau begins, decreases with the increase in temperature. This is due to the greater effectiveness of high-temperature environments in destroying quantum coherence. Secondly, we note that the plateau exists for a shorter length of time as the temperature is increased. This is because the increase in the plateau height due to the increase in temperature causes the entropy to approach its saturation value at an earlier time (by  $t = 8$  here). We note that the first of these features was mentioned by Zurek and Paz in the framing of their original conjecture [14]. They also expected a finite lifetime for the plateaux due to saturation effects. However, the increase of plateau height with temperature seen here shortens this lifetime still further, making the plateaux seem more and more like maxima as the temperature is increased.

For the highest temperature chosen, with  $\beta = 0.0001$ , we see that the initial coherence is lost so quickly as to render the dynamical localization mechanism ineffective. Indeed, a linear increase of  $\langle P^2(t) \rangle / 2$  with the time,  $t$ , is seen in figure [9] at this temperature, albeit at a lower rate than the classical value. This discrepancy, however, disappears as the temperature is increased still further. With regard to entropy and its production rate we see the above-mentioned features strikingly displayed: the entropy production rate has a maximum rather than a plateau; this maximum is greater than the plateaux heights of lower temperatures, and the maximum is reached at the shorter time of  $t = 3$ .

*4.2.2. Factors Affecting the Decay Probability* Evidence that increasing one or more of the temperature,  $\hbar$  and  $K$ , the magnitude of the kick, destroys the quantum coherence



more efficiently can be seen in figures [12] and [13]. There we have plotted the single-step decay probability,  $P_1$ , described in section 3 against  $K$ , for different temperatures (figure [12]) and values of the quantum of action (figure [13]). These figures clearly indicate that to destroy the dynamical localization mechanism more efficiently one should change these parameters in this way in order to reduce the coherence time,  $n_c$ . Furthermore, by increasing  $K$  and decreasing  $h$  we also increase the value of the break time,  $n^*$ , according to equation (18). This gives the environment “more time” to act as the situation  $n^* \gg n_c$  develops.

These observations are important in any consideration of the rate at which the system produces entropy. Entropy production in the system is a manifestation of the increase in phase space area (or volume for higher dimensional systems) that a wave packet occupies when it is perturbed by an environment. Localization, therefore, and the consequent restrictions this places on the extent to which this area can increase, *must* be considered as a factor which can affect the entropy. We note that the inverted oscillator model, notwithstanding its usefulness as a guide to intuition, cannot take this effect into account.

*4.2.3. The Modified Conjecture* In order to examine the validity or otherwise of the modified conjecture we plot, in figures [14] to [18], the constant rate of von Neumann entropy production,  $h_Q$ , versus the corresponding, classical, local KS entropy for given initial states, with different environmental parameters and values of the quantum of action.

In figure [14] we see a linear relationship but with *oscillations superimposed*. Here,  $h = 0.05\gamma$  and  $\beta = 0.10$ . Evidence that these oscillations have their origin in the dynamical localization mechanism can be gathered from the fact that the values of  $K$  at which the plot departs most from linear behaviour are precisely those values for which the quasilinear approximation to the classical diffusion coefficient,  $D(K)$ , is worst (see equation (9) and references [19, 23]). Thus, on account of the link between both the localization length,  $L$ , and the break time,  $n^*$ , given by equations (17) and (18), respectively, and the classical diffusion coefficient, we see that these values of  $K$  give rise to exceptionally small or large localization lengths and break times. This, for the reason given above, affects the rate of entropy production.

To investigate this effect further we have increased the temperature tenfold in figure [15], i.e.  $\beta = 0.01$ . We have also chosen to start initial minimum uncertainty states at five different points in phase space. Since the quasienergy eigenstates form a complete set, each initial state can be expanded in this basis and will have different expansion coefficients. Differing levels of importance will then be attached to the various basis states for each initial condition. Since the localization length varies from eigenstate to eigenstate we might therefore expect to see slightly different entropy production rates

for each such state, but with the linear behaviour still clearly in evidence. This is indeed the case. We also note that the slope of the graph has increased with the increase in temperature.

Running at higher temperatures when  $h = 0.05\gamma$  as in figures [14] and [15] quickly leads to undesirable saturation effects so we henceforth choose  $h = 0.1\gamma$  and examine the interplay between dynamical localization and the modified conjecture with this larger value for the quantum of action.

In figures [16], [17] and [18] we have done just that, but for values of the inverse temperature of  $\beta = 0.1, 0.001$  and  $0.0001$ , respectively. The starting point was chosen as  $(0.5, h)$ . Thus, the same parameter values are used here for values of  $K$  from  $3.5$  to  $\approx 25$  as were used in figures [9], [10] and [11] for  $K = 3$ . Figure [9], especially, should give one an indication of the increased effectiveness of a larger environmental temperature in destroying the dynamical localization. This is manifest in these figures. As the temperature is increased we see a transition from quite a poor linear relationship in figure [16] with large fluctuations due to the existence of a localization effect (especially for smaller  $K$  values) to obviously much better linear relationships in figure [17] and [18]. The fluctuations, though still present, are much reduced at these temperatures since there is now little or no localization to inhibit the spread of the evolving wave packet in the momentum direction. Once again we see that increasing the temperature has the effect of raising the slope.

## 5. Conclusion

We have shown that the rate of von Neumann entropy production for an initial state of the open quantum kicked rotor increases approximately linearly with the *local* KS entropy of a corresponding classical distribution. This approximation becomes more exact as the strength of the environment becomes great enough to destroy on a short enough timescale those quantum coherences which lead to dynamical localization in the absence of an environment. However, even in that “transition” region when the localization is just noticeably destroyed, linear behaviour is observed, albeit with localization-induced fluctuations superimposed.

We have also shown using this model, but believe it to be generally true given its prototypical nature, that: *a)* it is generally the case that the more classically chaotic a system is, the greater the rate its quantum counterpart will lose information to a perturbing environment; *b)* all system and environmental parameters being equal, different entropy production rates can still be seen depending on where one places the initial state in phase space. These locations correlate excellently with the classical mixed phase space structure, and finally; *c)* the constant rate of entropy increase depends very much on the nature and strength of the perturbing environment.

We note that observation *b*) here is not unique to the approach of coupling quantum chaotic systems to a thermal environment, as has been done here, or of otherwise perturbing it [36, 37]. Indeed, recently Mirbach and Korsch [38] have introduced a phase space entropy-like quantity,  $S(p, q)$ , which measures the (time averaged) spreading of minimum uncertainty wave packets centred initially at  $(p, q)$ . No environment is introduced in their approach. Contour plots of this quantity show increasing similarities to both the classical phase space structure of Poincaré sections of a harmonically driven rotor, and to a suitably defined *classical* phase space entropy, as  $\hbar$  is decreased. However, no connection is made with standard quantities used in the study of chaos, such as the KS entropy considered here.

These results, we speculate, provide good criteria by which to distinguish between the quantum mechanical counterparts of regular and chaotic classical motion in general, even in multi-dimensional systems.

## Acknowledgments

Paul A. Miller would like to thank the King's College London Association (KCLA) for a postgraduate studentship. We also thank Raphael Zarum for useful discussions.

## References

- [1] Casati G and Chirikov B V 1995 *Quantum Chaos* (Cambridge University Press)
- [2] Ozorio de Almeida A M 1988 *Hamiltonian Systems: Chaos and Quantization* (Cambridge University Press, New York)
- [3] Gutzwiller M C 1990 *Chaos in Classical and Quantum Mechanics* (Springer-Verlag, Berlin)
- [4] Haake F 1990 *Quantum Signatures of Chaos* (Springer-Verlag, New York)
- [5] Giannoni M J, Voros A and Zinn-Justin J eds. 1991 *Chaos and Quantum Physics*, Les Houches Lectures Session LII (North Holland, Amsterdam)
- [6] Berry M V 1987 *Proc. R. Soc.* **A413** 183
- [7] Korsch H J and Berry M V 1981 *Physica D* **3** 627
- [8] Ford J, Mantica G and Ristow G H 1991 *Physica D* **50** 493
- [9] Ford J and Ilg M 1992 *Phys. Rev.* **A45** 6165
- [10] Casati G, Chirikov B V, Izrailev F M and Ford J 1979 *Lecture Notes in Physics* vol 93 Casati G and Ford J eds. (Springer-Verlag, Berlin) 334
- [11] Sarkar S and Satchell J S 1988 *Physica D* **29** 343
- [12] Zurek W H 1993 *Prog. Theor. Phys.* **89** 281, and references therein.
- [13] Giulini D, Joos E, Kiefer C, Kupsch J, Stamatescu I O and Zeh H D 1996 *Decoherence and the Appearance of a Classical World in Quantum Theory* (Springer-Verlag, Berlin Heidelberg), and references therein.
- [14] Zurek W H and Paz J P 1994 *Phys. Rev. Lett.* **72** 2508; Casati G and Chirikov B V 1995 *Phys. Rev. Lett.* **75** 350; Zurek W H and Paz J P 1995 *Phys. Rev. Lett.* **75** 351; Zurek W H and Paz J P 1995 *Physica D* **83** 300

- [15] Miller P A and Sarkar S 1998 *Fingerprints of classical instability in open quantum dynamics*, to appear, *Phys. Rev.* **E**
- [16] Beck C and Schlögl F 1993 *Thermodynamics of Chaotic Systems* (Cambridge University Press)
- [17] Schack R and Caves C M 1996 *Phys. Rev.* **E53** 3257
- [18] Reichl L E 1992 *The Transition to Chaos in Conservative Classical Systems: Quantum Manifestations* (Springer-Verlag, New York)
- [19] Lichtenberg A J and Lieberman M A 1992 *Regular and Chaotic Motion* (Springer-Verlag, Berlin)
- [20] Moore F L *et al* 1995 *Phys. Rev. Lett.* **75** 4598
- [21] Ammann H, Gray R, Shvarchuck I and Christensen N 1998 *Phys. Rev. Lett.* **80** 4111
- [22] Chirikov B V 1979 *Physics Reports* **52** 263
- [23] Rechester A B and White R B 1980 *Phys. Rev. Lett.* **44** 1586; Rechester A B, Rosenbluth M N and White R B 1981 *Phys. Rev.* **A23** 2664
- [24] Pesin Y B 1977 *Russ. Math. Surveys* **32** No 4, 55
- [25] Fox R F and Lan B L 1990 *Phys. Rev.* **A41** 2952
- [26] Ott E, Antonsen Jr T M and Hanson J D 1984 *Phys. Rev. Lett.* **53** 2187
- [27] Cohen D 1994 *J. Phys. A: Math. Gen.* **27** 4805, and references therein.
- [28] Shiokawa K and Hu B L 1995 *Phys. Rev.* **E52** 2497
- [29] Caldeira A O and Leggett A J 1983 *Physica* **121A** 587 (1983)
- [30] Dittrich T and Graham R 1990 *Ann. Phys., NY* **200** 363
- [31] Dittrich T and Graham R 1986 *Z. Phys.* **B62** 515
- [32] Graham R 1985 *Z. Phys.* **B59** 75
- [33] Jiushu S, Mo-Lin G and Hu C 1996 *Phys. Rev.* **E53** 1243
- [34] Miller P A 1998 King's College London PhD thesis (unpublished)
- [35] Jensen J H and Niu Q 1990 *Phys. Rev.* **A42** 2513
- [36] Zarum R and Sarkar S 1998 *Phys. Rev.* **E57** 5467
- [37] Zarum R and Sarkar S 1998 *Global and local entropy measures of chaos for the quantum kicked top*, submitted to *Phys. Rev.* **E**
- [38] Mirbach B and Korsch H J 1995 *Phys. Rev. Lett.* **75** 362

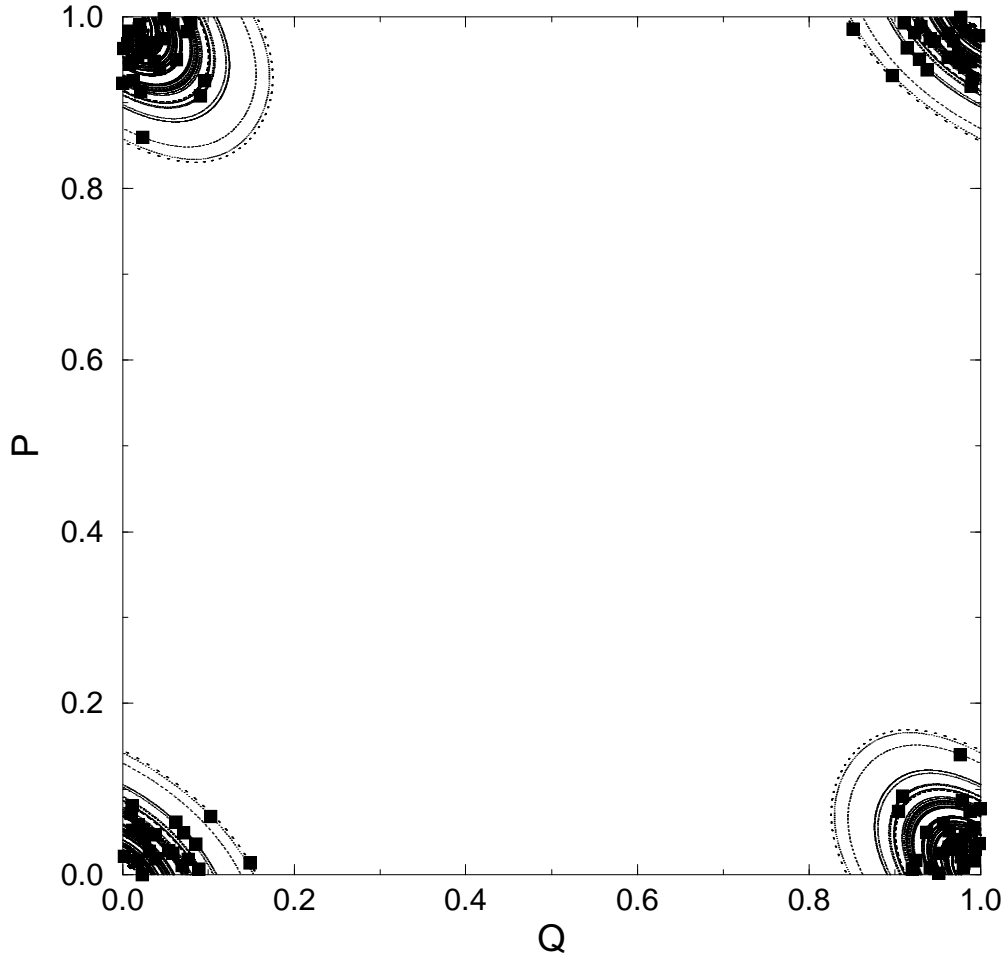


**Figure 1.** The squares are 100 sample points from an initial Gaussian distribution centred at the origin  $(0.0, 0h)$  with a variance of  $\hbar/2$  corresponding to a quantum initial state of minimum uncertainty. We choose  $\hbar = 0.05\gamma/(2\pi)$ . The dots mark the first 300 iterations of each such initial point, thereby giving an indication of the predominantly regular resultant trajectories.

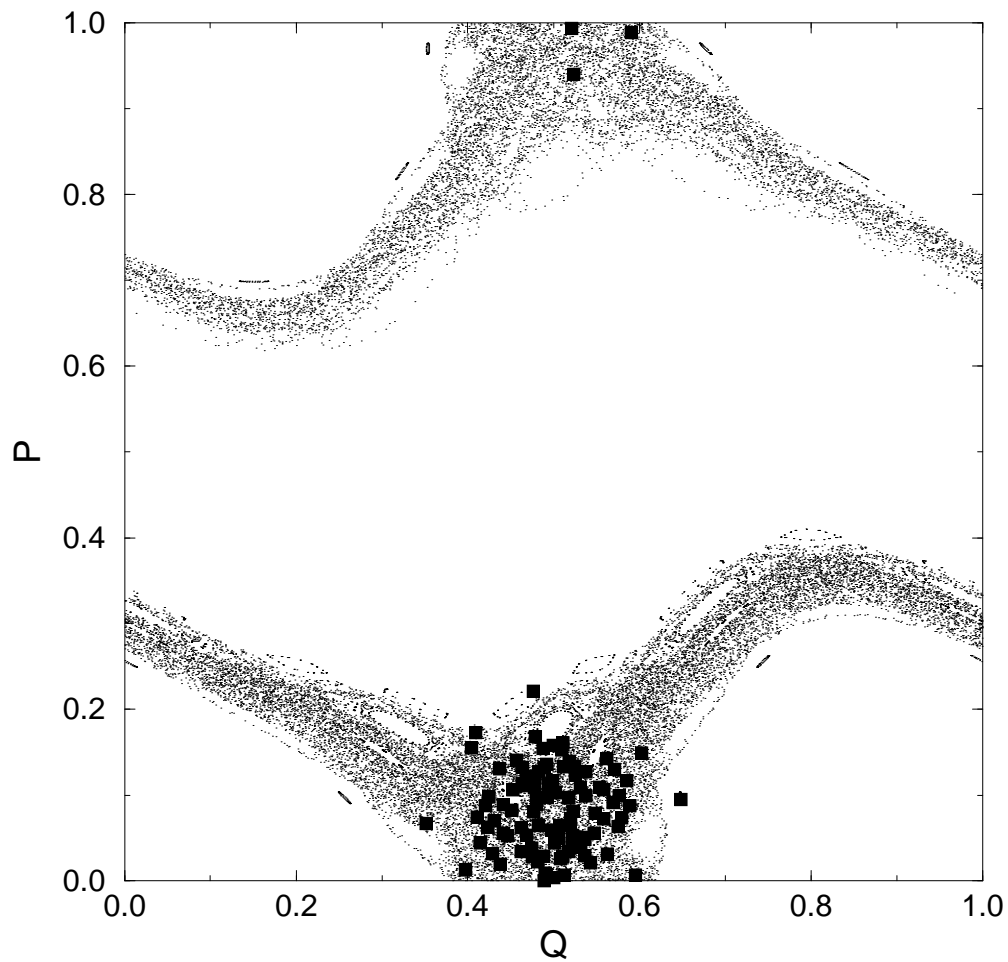


**Figure 2.** The squares are 100 sample points from an initial Gaussian distribution centred at  $(0.5, 2\hbar)$  with a variance of  $\hbar/2$  corresponding to a quantum initial state of minimum uncertainty. We choose  $\hbar = 0.05\gamma/(2\pi)$ . The dots mark the first 300 iterations of each such initial point, thereby giving an indication of the predominantly chaotic resultant trajectories.

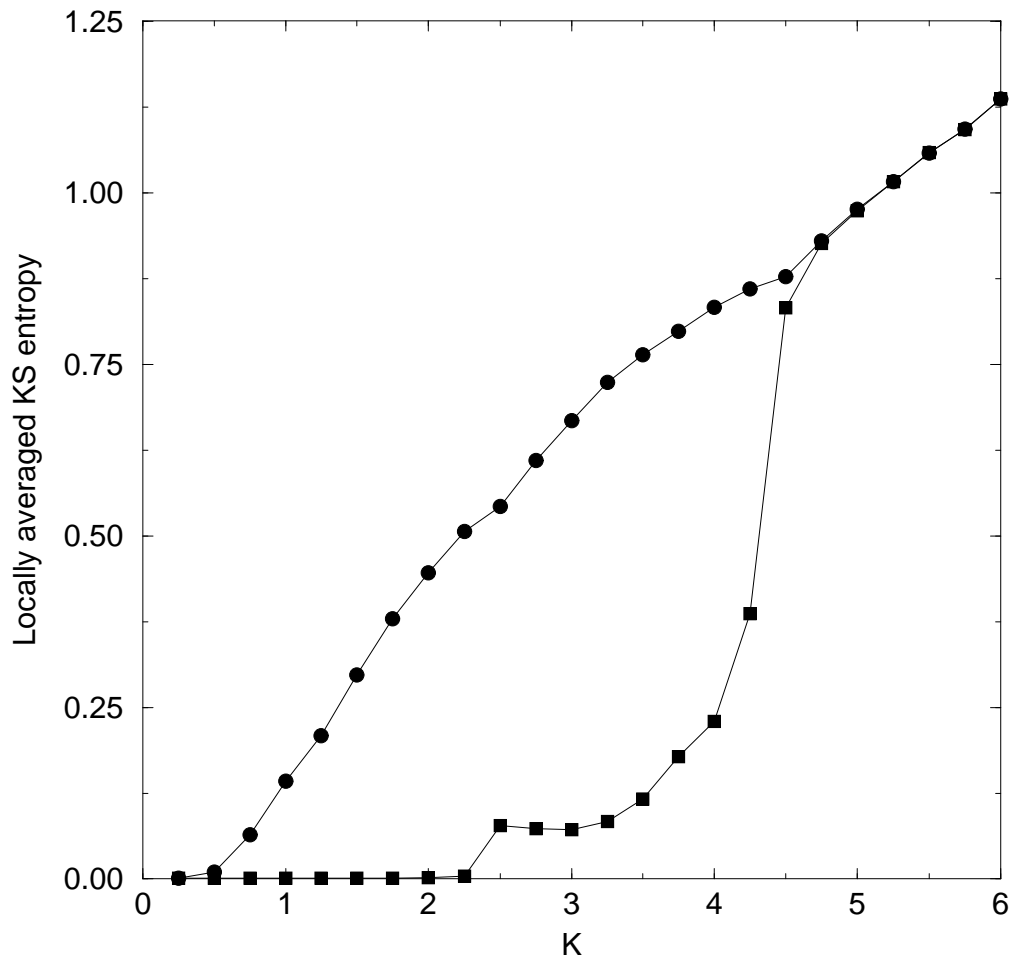


**Figure 3.** The locally averaged KS entropy of each distribution in figures [1] and [2], corresponding to the filled squares and the filled circles, respectively, plotted against  $K$ .

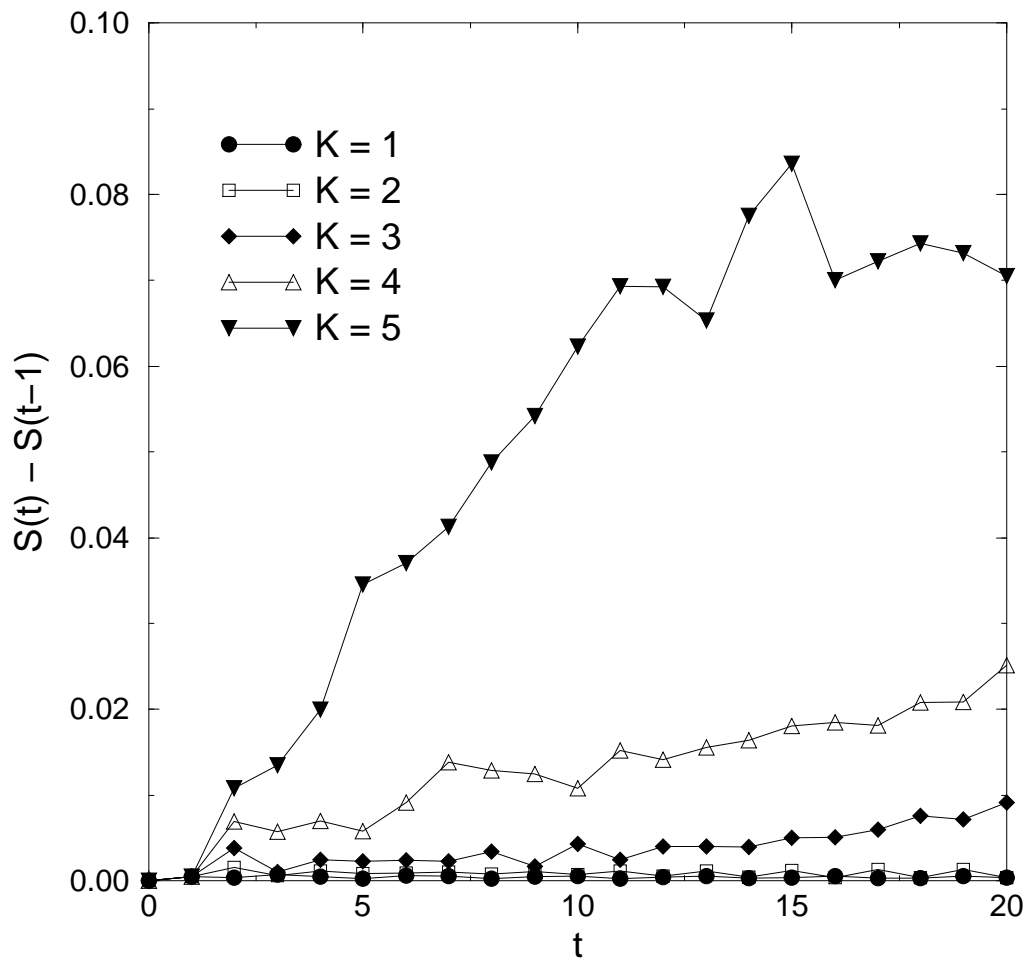


**Figure 4.** The change in the entropy production rate,  $h_Q$ , with time,  $t$ , for various values of  $K$ . The initial state corresponds to that plotted in figure [1], giving rise to regular trajectories. Parameter values used are  $h = 0.1\gamma, \beta = 0.1$ .



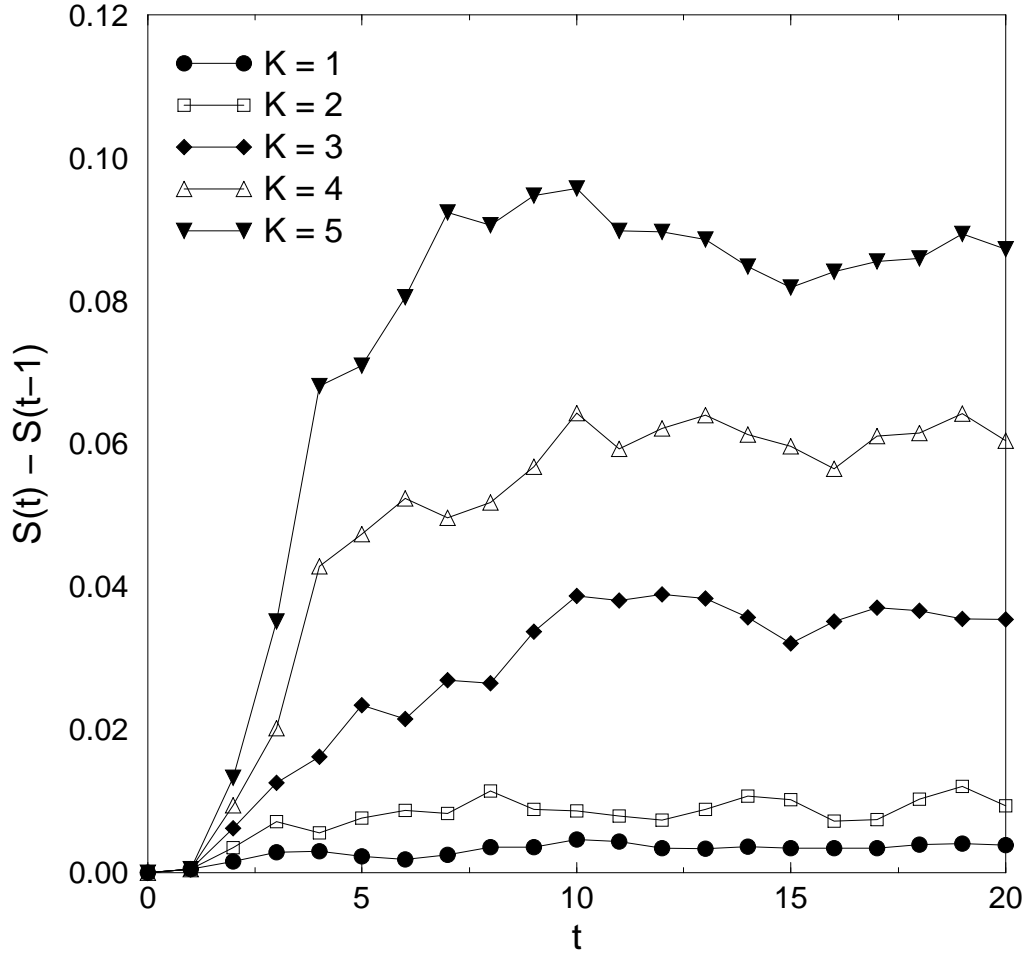


**Figure 5.** The change in the entropy production rate,  $h_Q$ , with time,  $t$ , for various values of  $K$ , and using the same parameter values of figure [4]. The initial state corresponds to that plotted in figure [2], giving rise to chaotic trajectories.

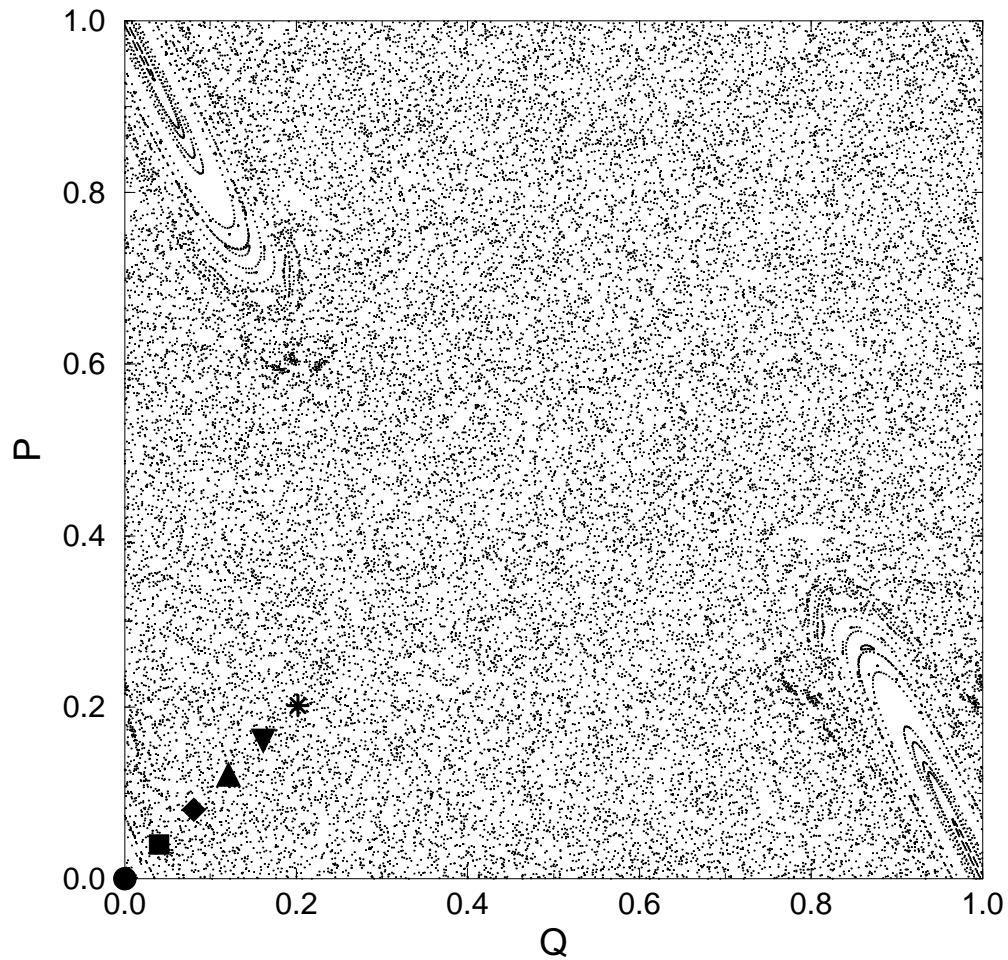


**Figure 6.** A classical phase space plot for  $K = 4$  with the stable island clearly visible. The superimposed symbols correspond to those in figure [7] and mark the centre of each initial coherent state for which the entropy rate is plotted in that figure.

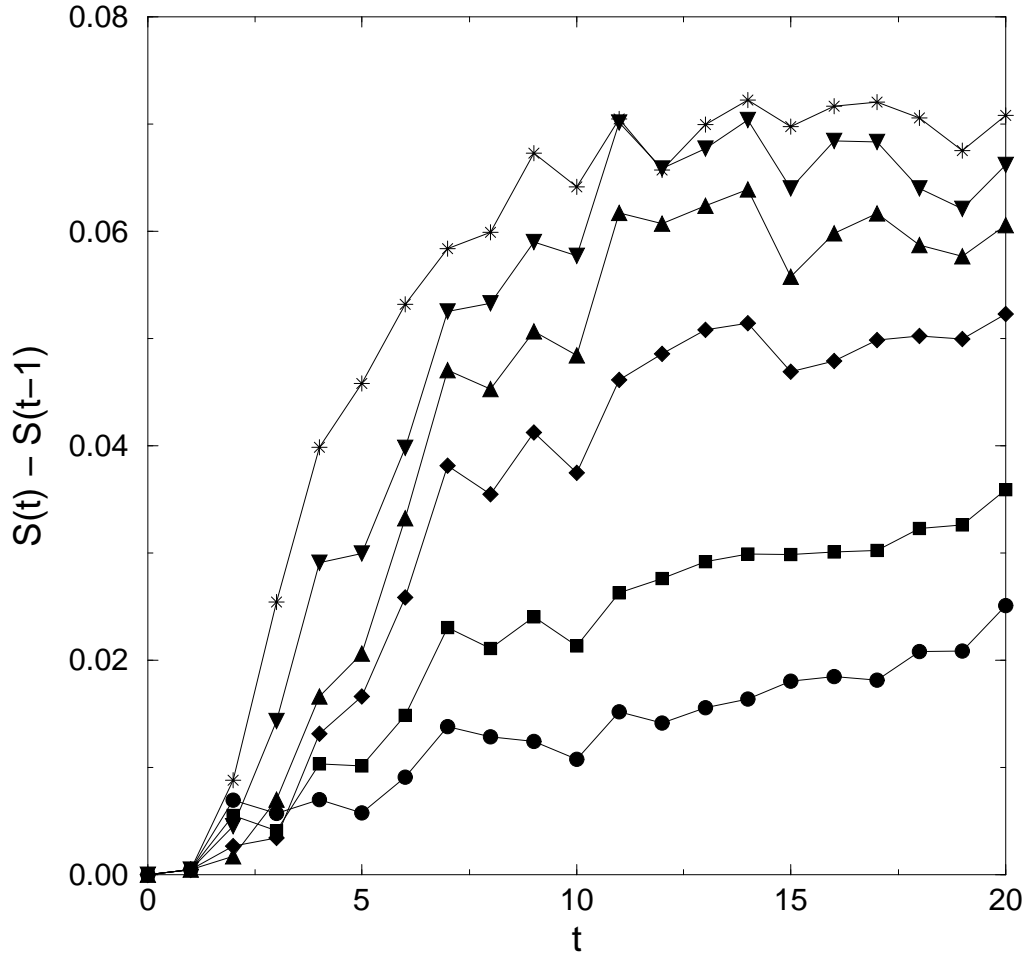


**Figure 7.** The rate of von Neumann entropy production for various starting points in the mixed phase space of figure [6] and denoted by the same symbols here. Here,  $h = 0.05\gamma$ .

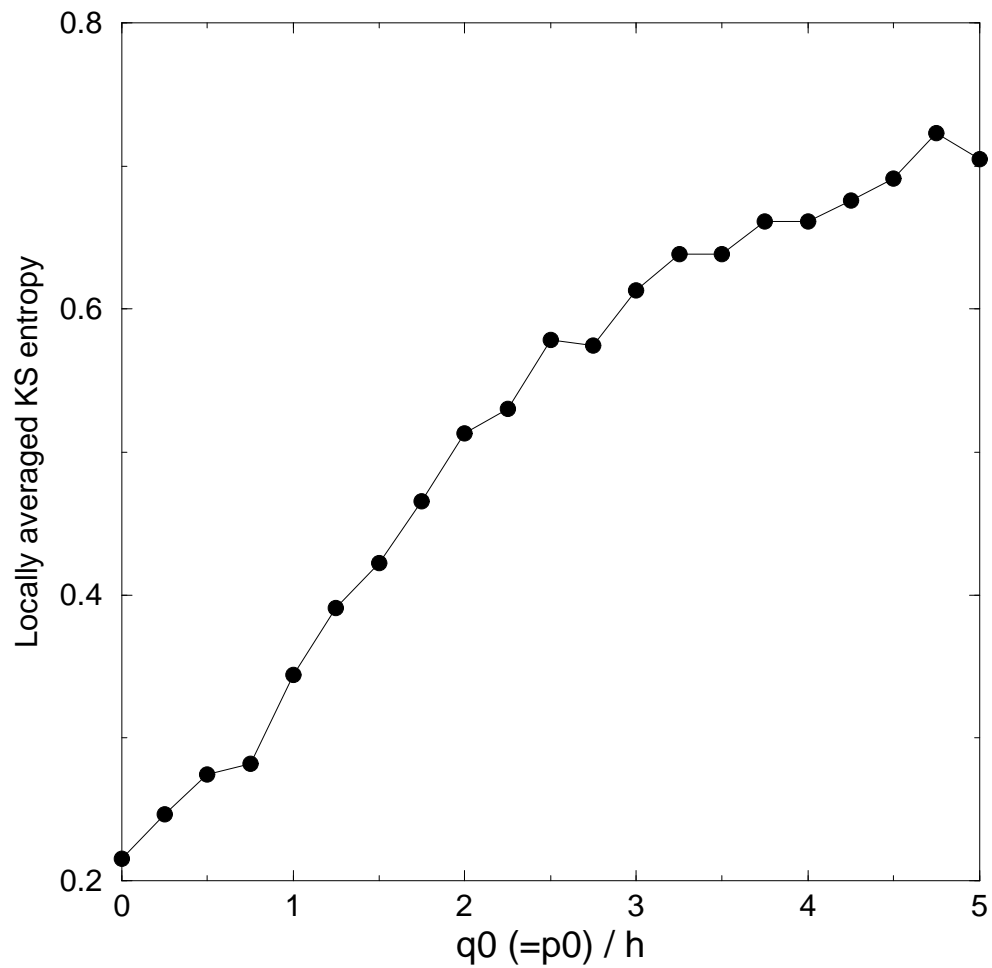


**Figure 8.** The classically calculated KS entropy for various initial Gaussian distributions centred along the diagonal  $q_0 = p_0$  in the mixed phase space of figure [6]. The position of the filled circles along the horizontal axis indicates the centre of the initial distribution. Again we choose  $h = 0.05\gamma$ .

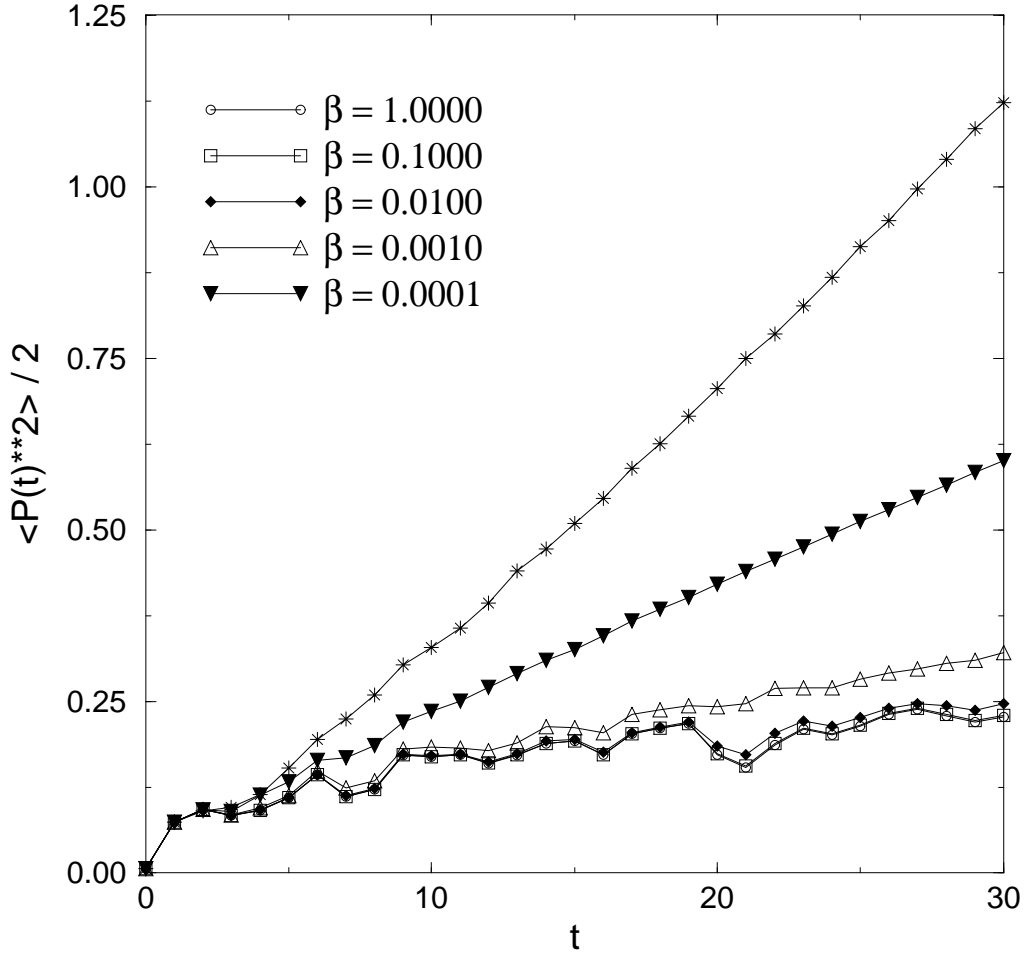


**Figure 9.** Here we see that increasing the temperature of the environment (equivalently, decreasing  $\beta$ ) has the effect of restoring the correspondence between quantum and classical expectation values. See the text for details.

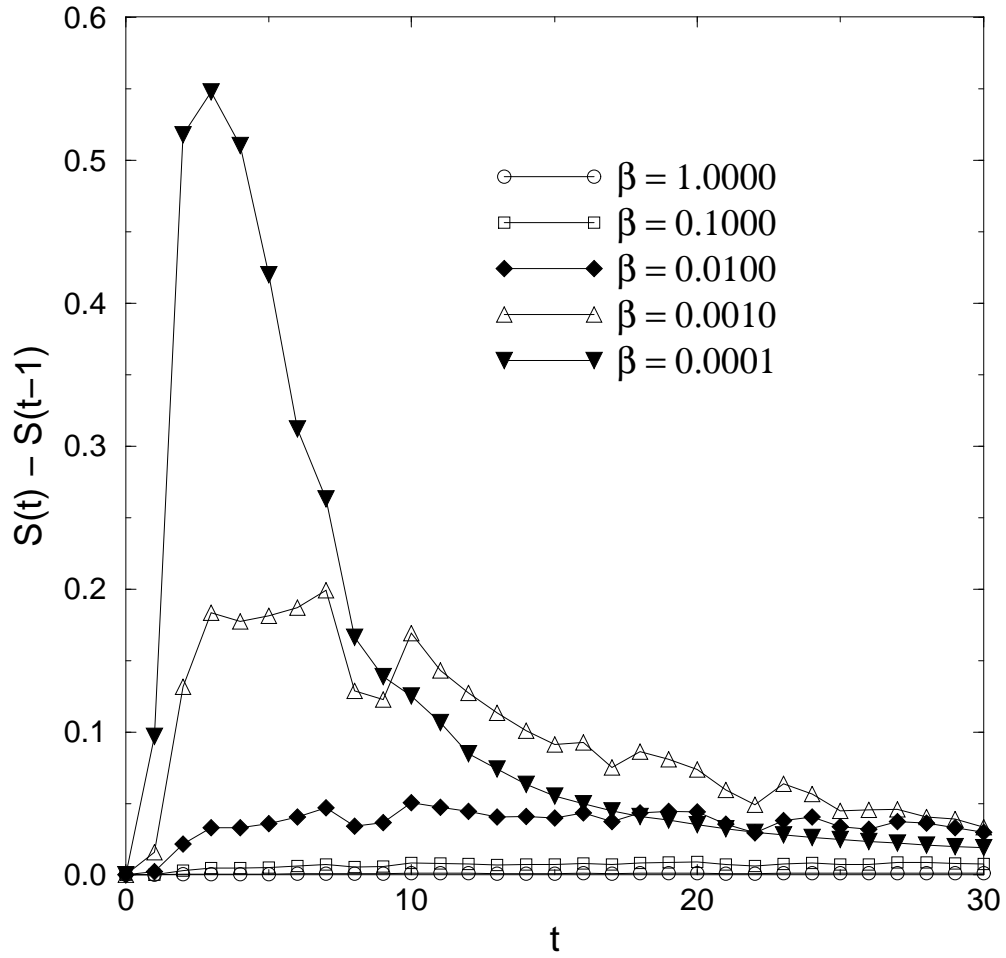


**Figure 10.** Here we see the consequences that restoration of the quantum-classical correspondence has for the von Neumann entropy production rate. See the text for details.

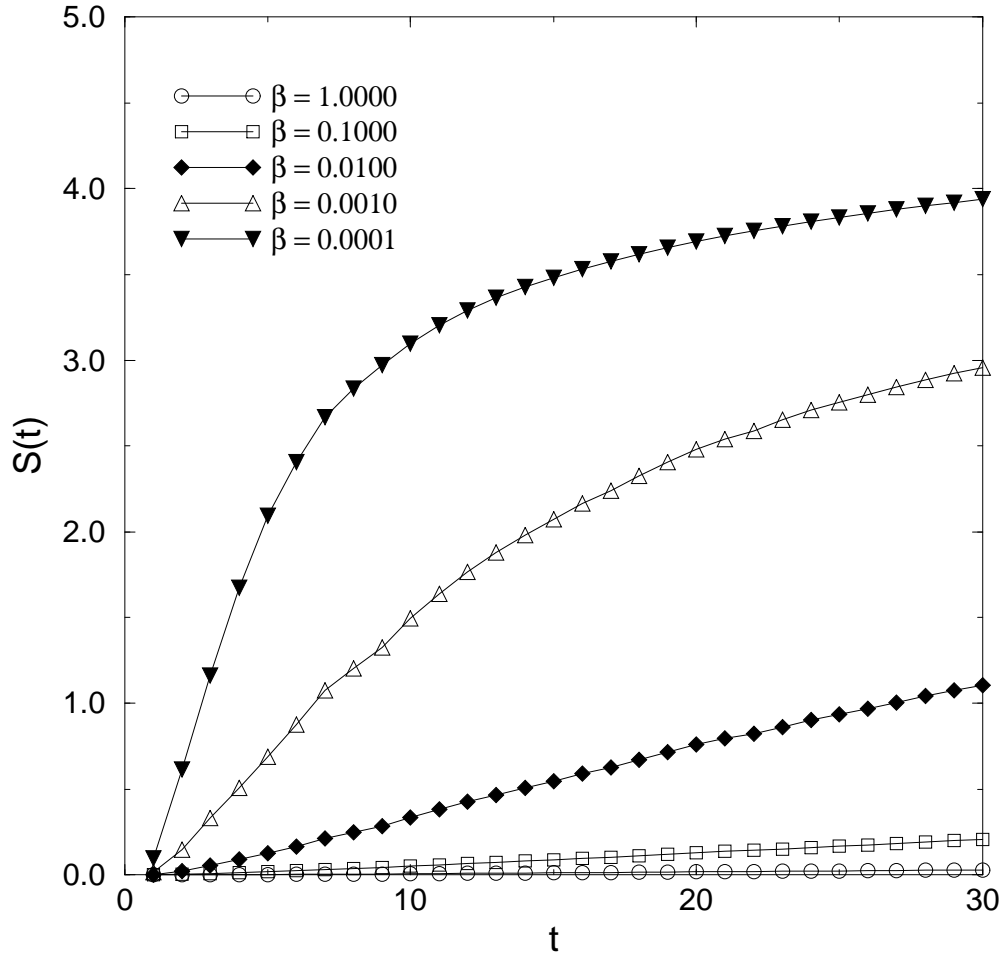


**Figure 11.** Here we see the consequences that restoration of the quantum-classical correspondence has for the von Neumann entropy. See the text for details.

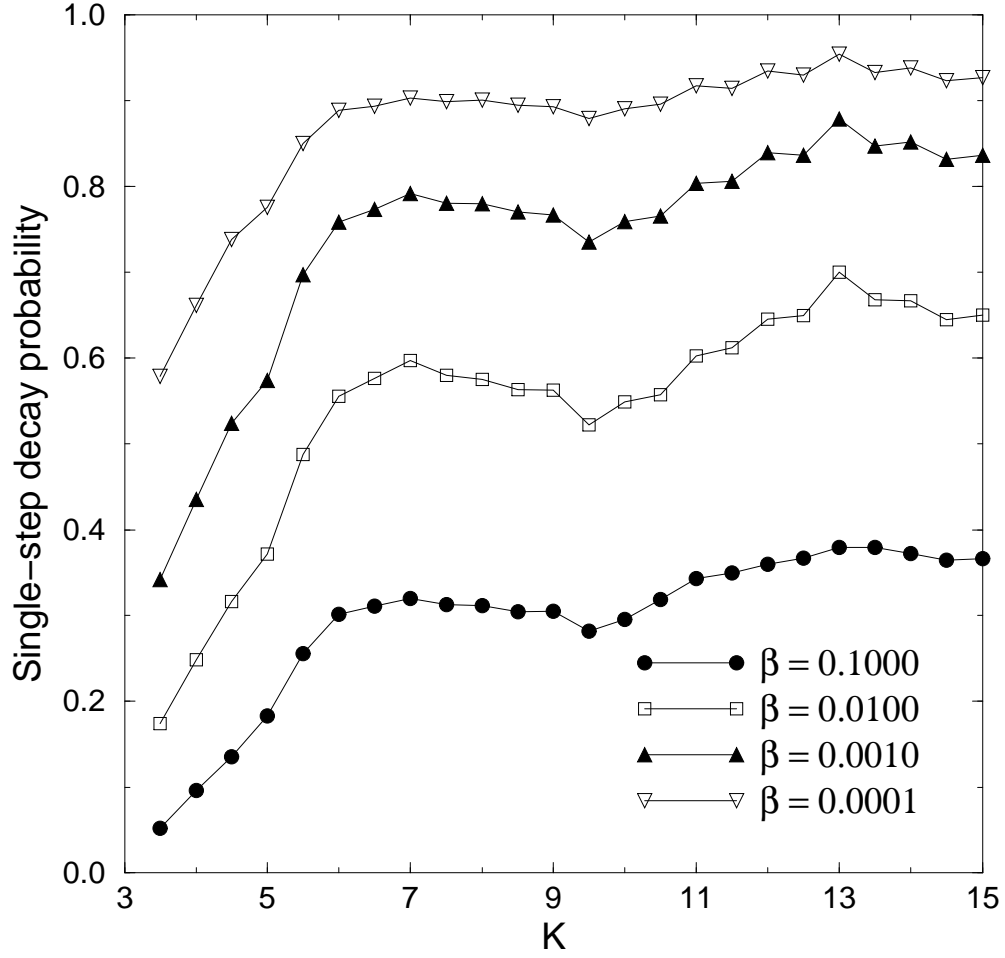


**Figure 12.** In this figure we plot the variation of the single-step decay probability,  $P_1$ , with  $K$ , for various different temperatures. We have chosen  $h = 0.1\gamma$ . See section 3 and section 5 for details.



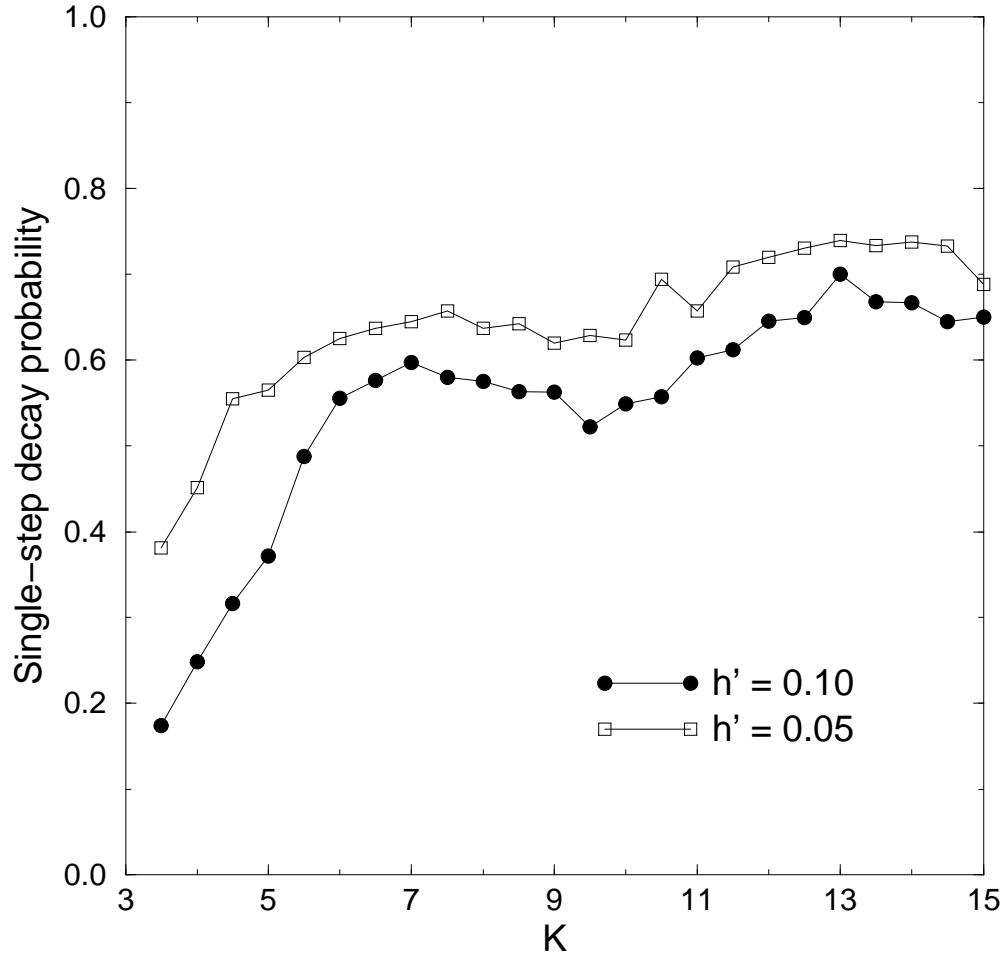


**Figure 13.** In this figure we plot the variation of the single-step decay probability,  $P_1$ , with  $K$ , for two different values of  $h$ . We have chosen  $\beta = 0.01$ . See section 3 and section 5 for details.

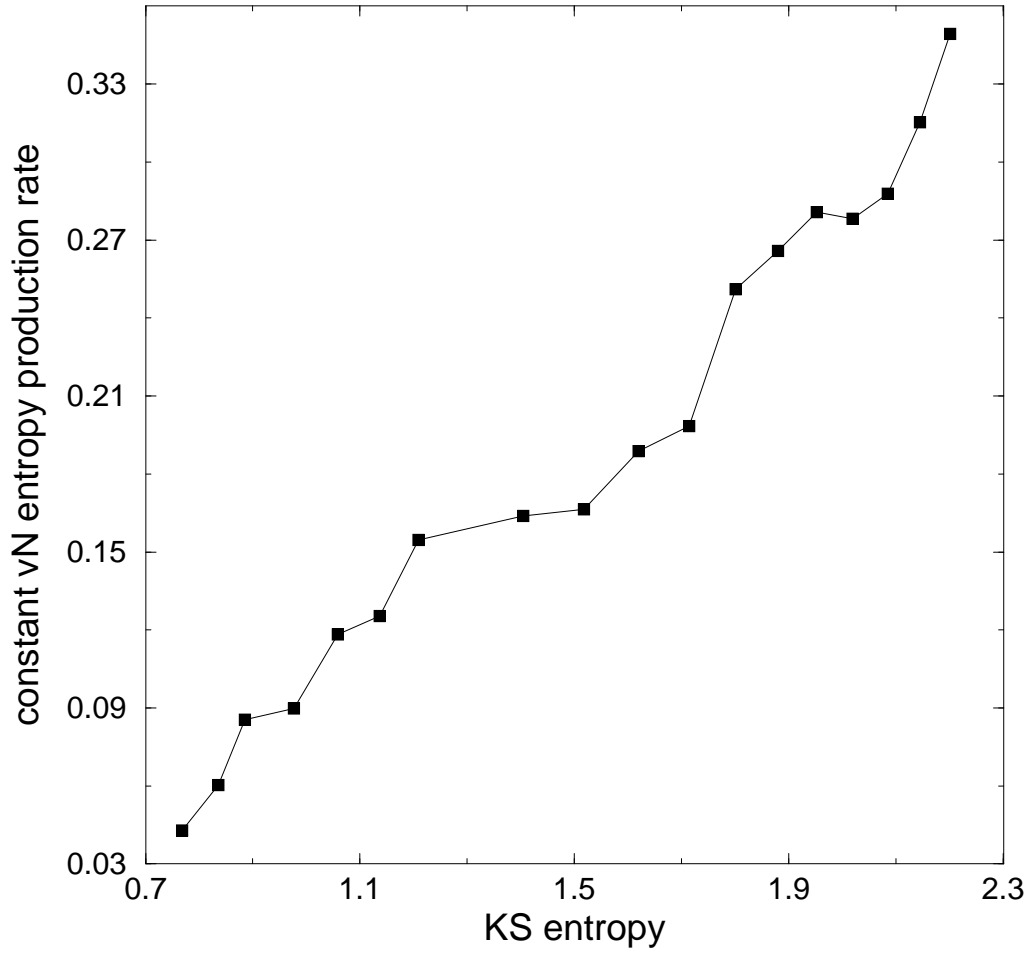


**Figure 14.** The constant entropy production rate plotted against the corresponding local KS entropy. The starting point in space is  $(0.5, 2h)$ , where  $h = 0.05\gamma$ . Here  $\beta = 0.1$ .

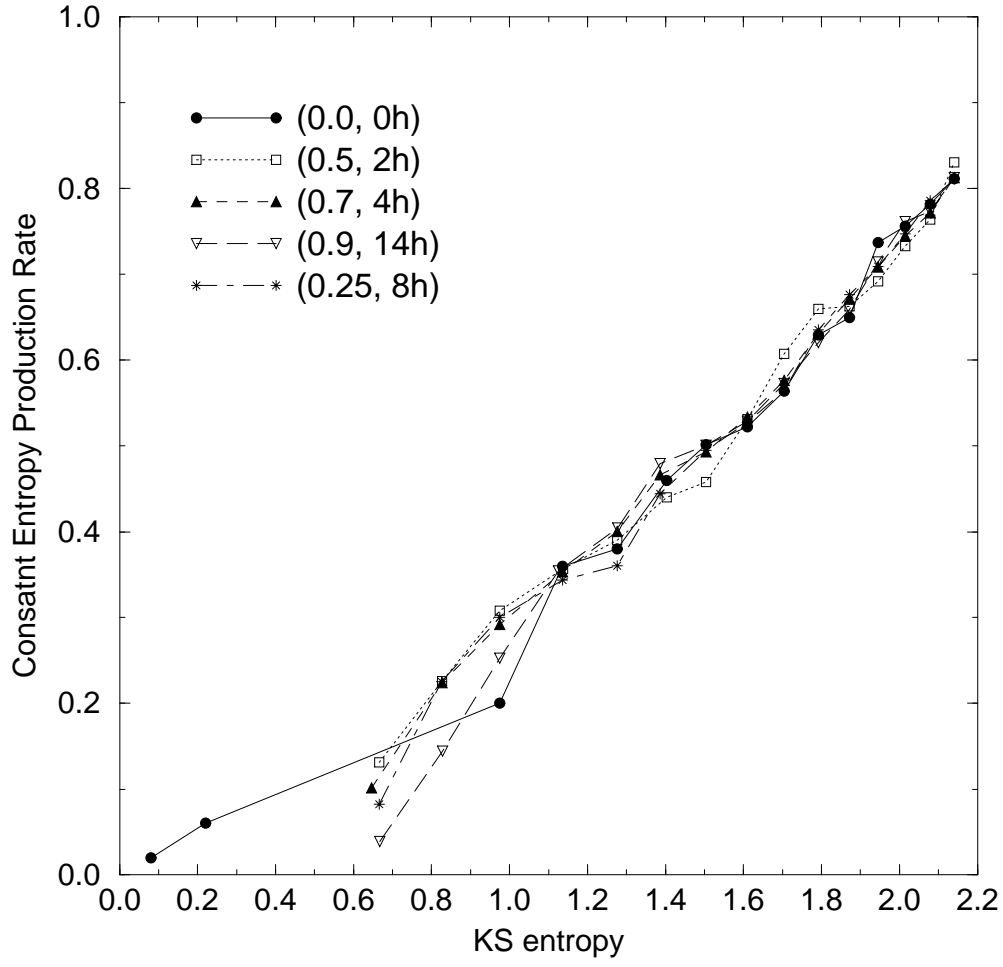


**Figure 15.** The constant entropy production rate plotted against the corresponding local KS entropy for five different starting points in phase space. Here, as in figure [12] we choose  $h = 0.05\gamma$  but  $\beta = 0.01$ .

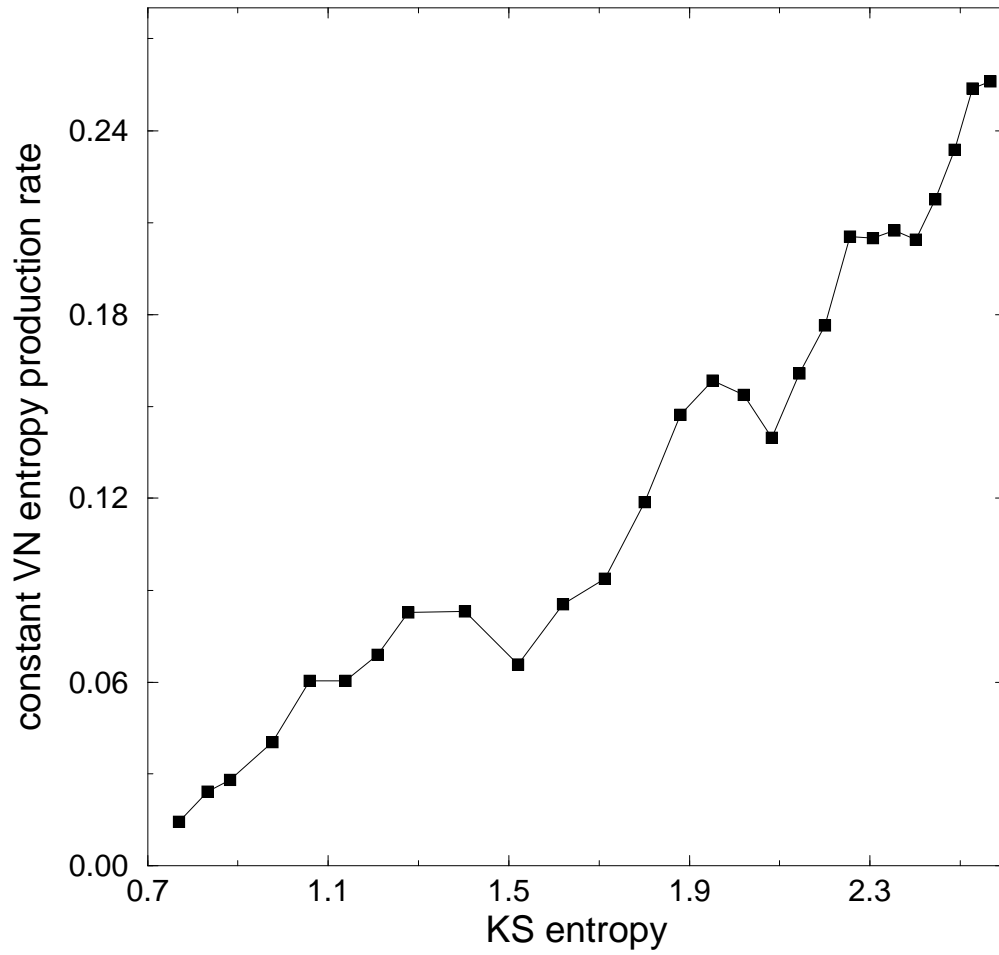


**Figure 16.** The constant entropy production rate plotted against the corresponding local KS entropy. The starting point in phase space is  $(0.5, h)$ , where  $h = 0.1\gamma$ . Here  $\beta = 0.1$ .

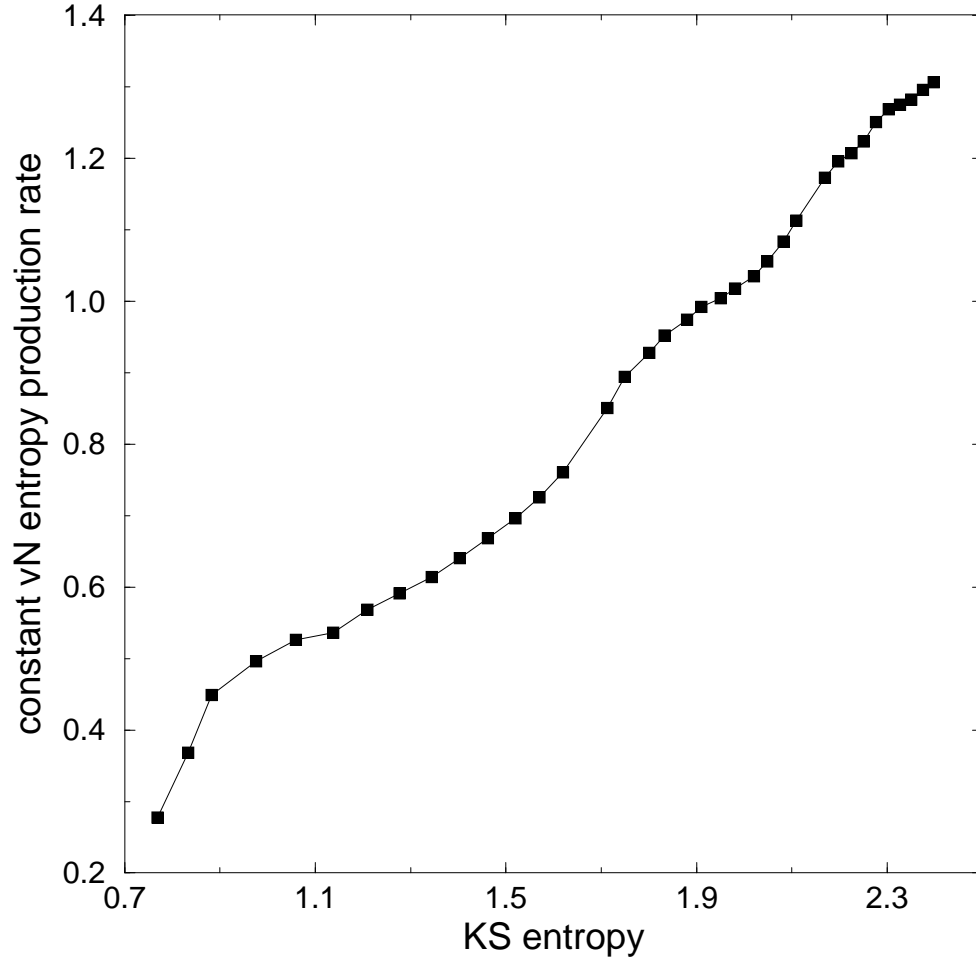


**Figure 17.** The constant entropy production rate plotted against the corresponding local KS entropy. The starting point in phase space is  $(0.5, h)$ , where  $h = 0.1\gamma$ . Here  $\beta = 0.001$ .

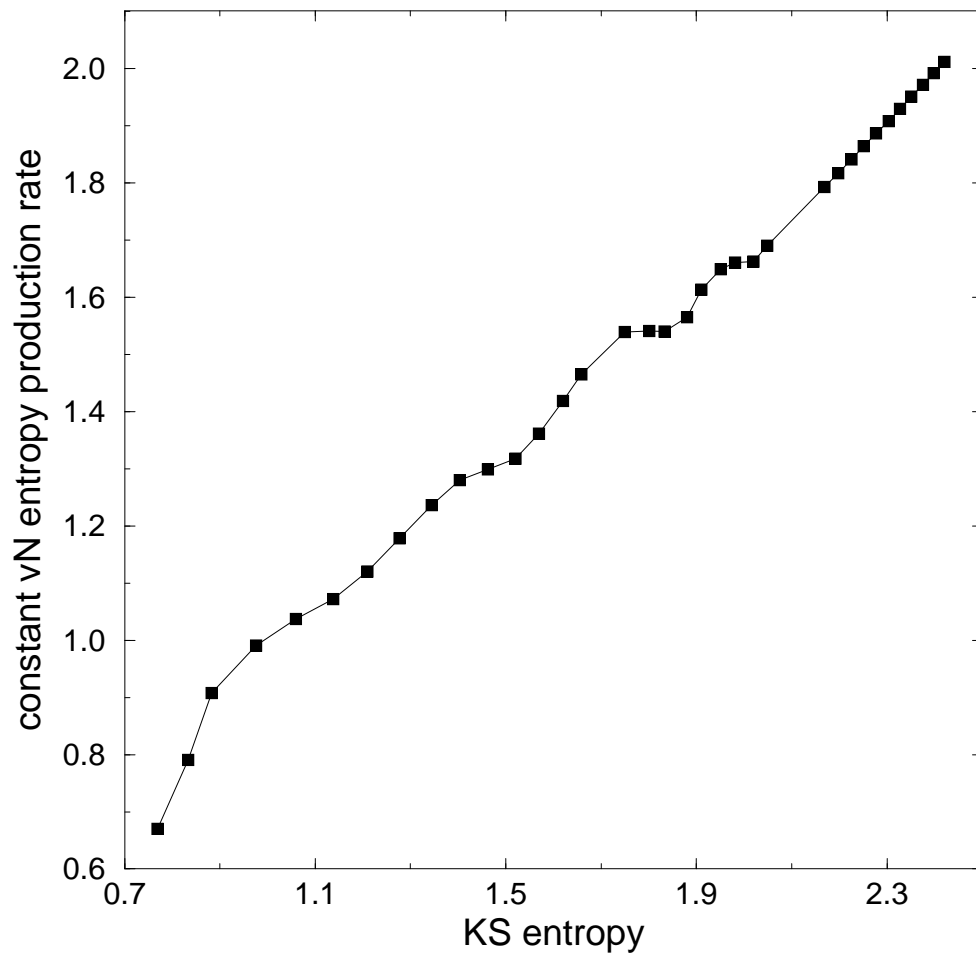


**Figure 18.** The constant entropy production rate plotted against the corresponding local KS entropy. The starting point in phase space is  $(0.5, h)$ , where  $h = 0.1\gamma$ . Here  $\beta = 0.0001$ .